Journal of Structural Geology, Vol. 15, No. 9/10, pp. 1223 to 1240, 1993
Printed in Great Britain

0191-8141/93 $06.00+0.00
Pergamon Press Ltd

Experimental dynamic metamorphism of mineral single crystals

STEPHEN H. KIRBY and LAURA A. STERN

Experimental Rock Mechanics Laboratory, Branch of Earthquake Geology and Geophysics, U.S. Geological Survey MS 977, 345 Middlefield Road, Menlo Park, CA 94025, U.S.A.

(*Received* 16 *September* 1992; *accepted in revised form* 22 *February* 1993)

Abstract—This paper is a review of some of the rich and varied interactions between non-hydrostatic stress and phase transformations or mineral reactions, drawn mainly from results of experiments done on mineral single crystals in our laboratory or our co-authors'. The state of stress and inelastic deformation can enter explicitly into the equilibrium phase relations and kinetics of mineral reactions. Alternatively, phase transformations can have prominent effects on rheology and on the nature of inelastic deformation. Our examples represent five types of structural phase changes, each of which is distinguished by particular mechanical effects. In increasing structural complexity, these include: (1) *displacive phase transformations* involving no bond-breaking, which may produce anomalous brittle behavior. A primary example is the α–β quartz transition which shows anomalously low fracture strength and tertiary creep behavior near the transition temperature; (2) *martensitic-like transformations* involving transformation strains dominated by shear deformation. Examples include the orthoenstatite → clinoenstatite and würtzite → sphalerite transformations; (3) *coherent exsolution* or precipitation of a mineral solute from a supersaturated solid-solution, with anisotropy of precipitation and creep rates produced under non-hydrostatic stress. Examples include exsolution of corundum from $MgO \cdot nAl_2O_3$ spinels and Ca-clinopyroxene from orthopyroxene; (4) *order–disorder* transformations that are believed to cause anomalous plastic yield strengthening, such as $MgO \cdot nAl_2O_3$ spinels; and (5) *near-surface devolatilization* of hydrous silicate single-crystals that produces a fundamental brittleness thought to be connected with dehydration at microcracks at temperatures well below nominal macroscopic dehydration temperatures.

As none of these interactions between single-crystal phase transformations and non-hydrostatic stress is understood in detail, this paper serves as a challenge to field structural geologists to test whether interactions of these types occur in nature, and to theoreticians to reach a deeper understanding of the complex relations between phase transformations, the local state of stress and associated deformation and deformation rates.

INTRODUCTION

DEFORMATION and metamorphism are fundamentally interrelated. For example, in regional metamorphism at convergent plate boundaries plate kinematics impose a flow field that changes pressures and temperatures such that mineral assemblages are placed outside their fields of thermodynamic stability while being deformed. Where these changes of state involve fluids, fluid migration in general probably requires the active tectonic maintenance of fracture permeability because such permeability is likely to disappear rapidly by fracture healing and mineral deposition in the absence of tectonic stresses (e.g. Smith & Evans 1984). Even under macroscopically hydrostatic stress, grain-scale conditions are generally non-hydrostatic due to differences in thermal expansion and elastic properties in polymineralic rocks and due to anisotropy in these properties even in single-phase rocks. Heterogeneous volume changes also produce grain-scale deviatoric stresses (e.g. Wheeler 1987, Green & Burnley 1989).

Even though development of theories of phase changes under deviatoric stress extends back at least to the time of J. W. Gibbs, there have been few experimental studies of phase changes in minerals to constrain theory. This paper summarizes some of the interactions that have been observed between phase changes, stress and deformation of mineral single crystals, mainly drawn from experiments with which we have been involved. Several of these experimental studies were done for other purposes, and we accidently stumbled into the effects of phase changes.

This work cannot be considered a comprehensive review but rather is intended to call attention of field geologists to some of the effects of phase changes observed in single crystals, to stimulate additional experimental studies of this type and to encourage theoretical developments to help understand these complex phenomena. Reviews of the physics and chemistry of phase changes and mineral reactions may be found in the following: Heuer & Nord (1976), Putnis & McConnell (1980), Porter & Easterling (1981), Rubie & Thompson (1985) and Lorimer (1988). Most of the work in the last decade exploring the effects of metamorphic reactions on rock rheology has focused on the roles of reduced grain size and dehydration (White & Knipe 1978, Beach 1980, Rubie 1983, 1990, Brodie & Rutter, 1986, 1987, Rutter & Brodie 1988). The present paper is restricted to metamorphic processes that occur primarily in grain interiors. This is not to imply that grain-boundary processes are not important in these phenomena, but that the study of single crystals in isolation from grain-neighbor constraints is an important first step.

The spectrum of interactions between phase changes, local and macroscopic states of stress, and inelastic deformation (and deformation rates) is potentially very complex, and is illustrated schematically in Fig. 1. Part of this complexity stems from the fact that transformations and mineral reactions are heterogeneous both on the field scale (due to variations in pressure, tempera-

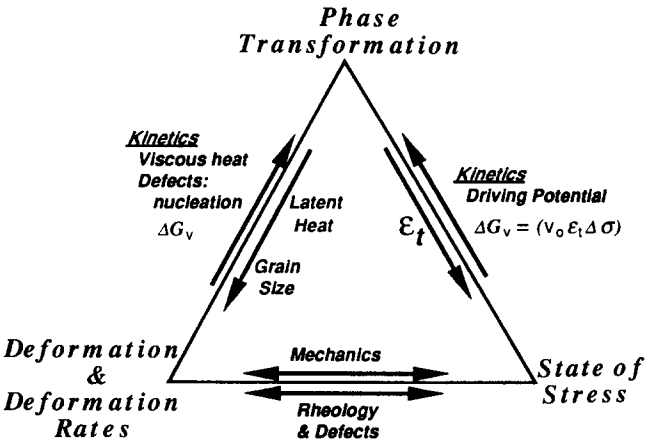

Fig. 1. Schematic overview of the interactions between phase changes, local and macroscopic states of stress, and inelastic deformation. Symbols: ε_t is the transformation strain tensor, ΔG_v is the Gibbs free energy difference between the product and the parent phase(s) and $\Delta\sigma$ is the overstep of the stress tensor from equilibrium pressure P_o at temperature T_o

ture or fluid activity) and on the microscopic scale (associated with the specific nucleation mechanisms). Consequently, both grain-scale and macroscopic states of stress can be altered through the transformation strain.

The effect of the macroscopic state of stress on the stability of *coherent* polymorphs is most explicit. Coherent polymorphs are those for which there are specific crystallographic rules by which the polymorphs are related. The transformation strain tensor ε_{ij}^T is specified by these rules. Structural continuity is maintained along the interphase boundary and hence the parent phase must accommodate the transformation strain of its product phase. A good example of the influence of non-hydrostatic stress on a coherent phase change is the α–β quartz transformation. Figure 2 shows how normal stress parallel to [0001] and normal to [0001] affects the stabilities of the two polymorphs. The slopes of the phase boundaries in these two principal directions are different because the transformation strains differ with direction. This may be made explicit by writing the expression for the change in Gibbs free energy $\Delta G^{\alpha-\beta}$ in terms of the tensor products of stresses σ_{ij} and transformation strains $\Delta\varepsilon_{ij}$ instead of the product of pressure and transformation volume change as in the hydrostatic stress case:

$$\Delta G^{\alpha-\beta} = \Delta H^{\alpha-\beta} - T\Delta S^{\alpha-\beta} - v_o \sigma_{ij} \Delta\varepsilon_{ij}^{\alpha-\beta}, \qquad (1)$$

where v_o is the molar volume of α quartz, $\Delta H^{\alpha-\beta}$ is the change in enthalpy at zero stress, $\Delta S^{\alpha-\beta}$ is the change in entropy at zero stress, and the products of transformation strain and stress are summed over the indices i and j. It is assumed here that the transformation strain tensor is, to first order, independent of stress. The last term is a work term that is the counterpart of pressure–volume work under hydrostatic conditions. As pointed out by Coe (1970) and Paterson (1973), care must be taken in defining $\Delta\varepsilon_{ij}$ and σ_{ij} such that their product properly represents the work term represented in $\Delta G|_T$ for transformations that have large finite transformation strains. Rewriting equation (1) in terms of the oversteps of the equilibrium lines between parent phase 1 and product phase 2,

$$\Delta G^{1-2}|_{P_o,T_o} = -v_o^1 \Delta\sigma_{ij} \Delta\varepsilon_{ij}^{1-2}, \qquad (2)$$

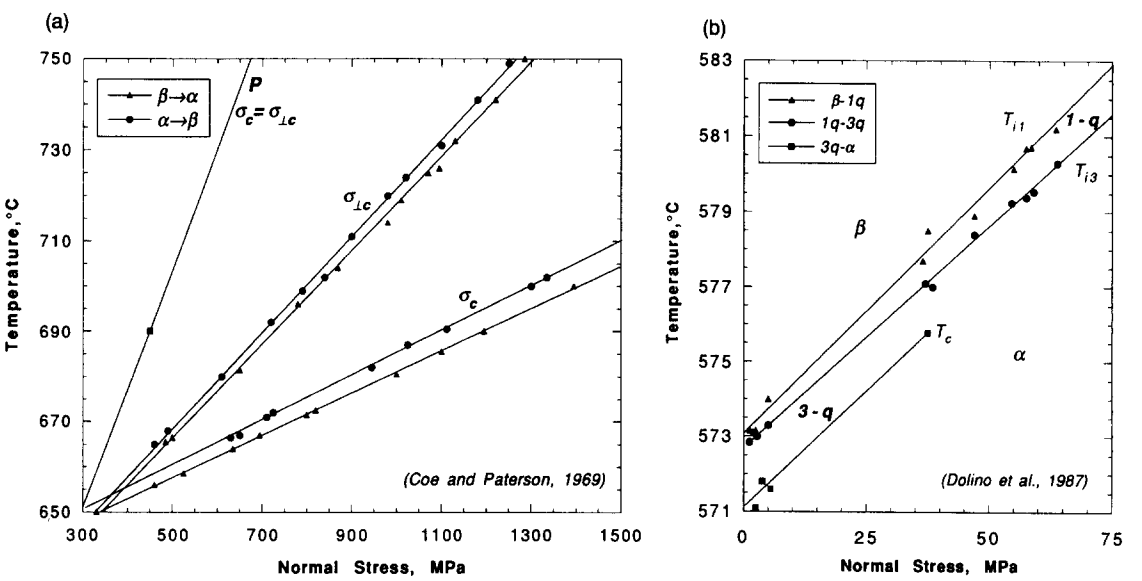

Fig. 2. (a) Phase diagram of the α–β quartz transition temperature at 300 MPa confining pressure as a function of pressure and compressive normal stress $\perp$c and $\|$c, after Coe & Paterson (1969). This illustrates the effect of normal stress orientation on the phase boundary between the two polymorphs. The transition $\beta \rightarrow \alpha$ (increasing stress) is denoted by triangles and $\alpha \rightarrow \beta$ (decreasing stress) by circles. The hydrostatic boundary P designates the α–β transition at zero compressive stress (Cohen & Klement 1967). Note the markedly steeper effect of compressive stress normal to c compared to that parallel to c. (b) Phase diagram of quartz under compressive stress $\perp$c, after Dolino *et al.* (1987), showing the presence of the two incommensurate phases $1q$ and $3q$ which form first-order and second-order phase boundaries, respectively, with α and β over about a 2°C temperature interval. Phase identification by *in situ* synchrotron X-ray diffraction. The $3q$ phase represents all three symmetrically equivalent pairs of Dauphiné twins whereas $1q$ has a single pair of twin orientations. Triangles, circles, and squares correspond, respectively, to the β–$1q$, $1q$–$3q$, and $3q$–α transition points. Same ratio of scales as (a), indicating that the phase boundaries are parallel to those determined by Coe & Paterson (1969) in the $\perp$c compression direction.

where $\Delta\sigma_{ij}$ is the stress overstep where the pressure corresponds to the equilibrium pressure P_o at temperature T_o, and the transformation strain, $\Delta\varepsilon_{ij}^{1-2}$, is assumed to be independent of the magnitude of stress. Equilibrium phase relations can be established with stress as the intensive variable. Expressions equivalent to the Clapeyron relation may be written:

$$(d\sigma_{ij}/dT)_{eq} = \Delta S/v_o\Delta\varepsilon_{ij} \quad (3)$$

and give the slope of the equilibrium line in σ_{ij}–T space as the ratio of the change in entropy and the transformation strain $\Delta\varepsilon_{ij}$. This relationship shows explicitly that the greater the transformation strain in a given crystallographic direction, the bigger the effect of stress on the equilibrium temperature (Fig. 2).

Equation (2) is important because it is a general expression for the driving potential for the kinetics of reactions. It also establishes the basic energetics of transformation, because $\Delta G^{1-2}|_{P_o,T_o}$ is the maximum work that can be extracted from a transformation, and is the source of elastic strain energy stored in the system microscopically associated with nuclei or inclusions of the new phase, stored as macroscopic stresses, dissipated as viscous heat, or bound up in crystal defects such as dislocations and grain boundaries. The potential interactions between the macroscopic stress state, the stress state on a grain scale, phase transformations, deformation and deformation rates suggested by Fig. 1 are rich and complex. For example, grain size reduction and the release of latent and dissipated heat associated with transformations and mineral reactions have important potential implications for the ductile rheology of rocks.

We now turn to specific laboratory examples of some of these interactions, progressing from the simplest transformations to the more complex.

DISPLACIVE PHASE TRANSFORMATIONS; THE α–β QUARTZ TRANSITION

Displacive phase changes constitute a relatively simple type of structural transformation, as they involve no bond breaking and only minor shape change. Under deviatoric stress, minerals undergoing displacive transformations potentially may produce anomalous behavior near their transition temperatures (Table 1). Quartz

Table 1. Displacive phase transformations in rock-forming minerals

Mineral (formula)	Space Groups $T<T_C$ $T>T_C$	T_C, K	P, MPa	Intermediate Phases and Related Structures	References
Quartz SiO_2	$(\alpha)\ P3_221 \leftrightarrow (\beta)\ P6_222$ $P3_121 \leftrightarrow P6_422$	846	0.1	Incommensurate *3q* and *1q*; Dauphiné twins	Dolino (1988)
Berlinite $AlPO_4$	$(\alpha)\ P3_221 \leftrightarrow (\beta)\ P6_222$ $P3_121 \leftrightarrow P6_422$	856	0.1	Incommensurate *3q* and *1q*; Dauphiné twins	Dolino (1988)
Cristobalite α-SiO_2	$(\alpha)\ P4_12_12 \leftrightarrow (\beta)\ Fd\bar{3}m$ $P4_232$	523 - 535		{112} twins	Thompson & Wennemer (1979)
Tridymite α-SiO_2	$(\alpha)\ C_c$ *or* $C2/c \leftrightarrow (\beta)\ P2_12_12_1$ (and others)	383 - 390 423, 463, 653			Thompson & Wennemer (1979), Cohen & Klement (1980), Nukui *et al.* (1978)
Anorthite $CaAl_2Si_2O_8$	$P\bar{1} \leftrightarrow I\bar{1}$	516	0.1	APB structure	Ghose *et al.* (1988), Angel (1988)
Sanidine $(K,Na)AlSi_3O_8$	$C\bar{1} \leftrightarrow C2/m$	273	2400.0		Hazen (1976)
Albite $NaAlSi_3O_8$	$C\bar{1} \leftrightarrow C2/m$	978	0.1		Kroll *et al.* (1980), Hazen (1976)
Larnite Ca_2SiO_4	$\alpha'_L = Pcan \leftrightarrow \alpha'_H = Pcmn$	1433			Kriven (1988)
Åkermanite $Ca_2(Mg,Fe)Si_2O_7$	$P\bar{4}2_1m \leftrightarrow P\bar{4}2_1m$	357		Incommensurate	Hemingway *et al.* (1986), Seifert *et al.* (1987)
Tungstite WO_3	$P4/nmm \leftrightarrow Pm\bar{3}n$	1173	0.1		Sirotin & Shaskolskya (1982)
Calcite $CaCO_3$	$I = P2_1/c$ $II = R\bar{3}c$	296	1500.0		Merrill & Bassett (1975)
Soda-niter $NaNO_3$	$R\bar{3}c \leftrightarrow R\bar{3}m$	553	0.1		Reeder *et al.* (1988)
Leucite $KAlSi_2O_6$	$(\alpha)\ I4_1/a \leftrightarrow I4_1/acd$ $I4_1/acd \leftrightarrow (\beta)\ Ia\bar{3}d$	918 938	0.1 0.1	Twin plane = contact = $\{101\}_T$	Lange *et al.* (1986), Palmer *et al.* (1988, 1989)
Mg-Cordierite $Al_3Mg_2(Si_5Al)O_{18}$	$Cccm \leftrightarrow P6/mcc$	1723	0.1	"Modulated structure"	Langer & Schreyer (1969)
Clinoenstatite $(Mg,Fe)SiO_3$	$P2_1/c \leftrightarrow C2/c$	1253	0.1		Smith (1969), Smyth & Burham (1972)

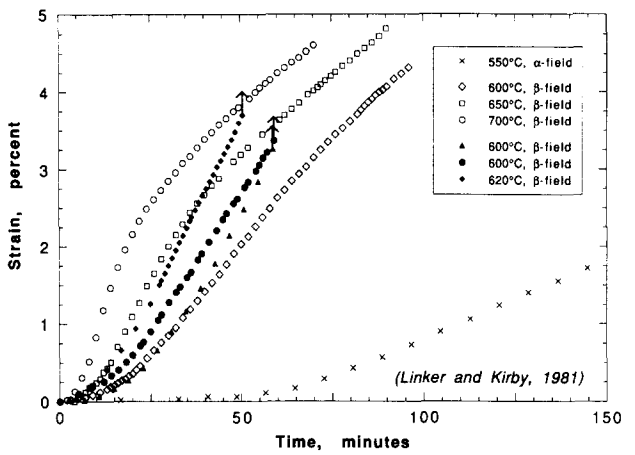

Fig. 3. Creep of crystallographically-oriented synthetic quartz single crystals at 140 MPa confining pressure and temperatures of 550–700°C, after Linker & Kirby (1981). In three samples compressed at 45° to [0001] and [1210] at 600 and 620°C (designated by solid symbols), strain rates were unusually high compared to samples compressed in the same orientation at higher or lower temperatures (open symbols). The three samples exhibiting anomalous behavior eventually failed catastrophically by fracture (upward arrows).

undergoing the α–β transition serves as a primary example, displaying low fracture strength and tertiary creep behavior.

It is well known that quartz is very sensitive to thermal shock, and workers in quartz technology have long been aware that quartz is particularly susceptible to thermally induced fracturing when cooled through the α–β transition. Less well known is that anomalously low fracture strength and brittleness occur in quartz even under nominally isothermal conditions near the α–β transition. Linker & Kirby (1981) examined the creep of oriented synthetic quartz crystals. Over most temperatures in the range 400–800°C, large plastic strain was sustained by the specimens with uniaxial stresses in the range 80–160 MPa. In crystals compressed at 45° to [0001] and $[2\bar{1}\,\bar{1}0]$ over a narrow range of temperature $550°C < T < 650°C$, strain rates were notably higher compared to samples deformed at higher or lower temperatures (Fig. 3) and three samples eventually failed catastrophically by fracture. Two samples that were unloaded prior to macroscopic failure were riddled with microfractures. Another suite of samples compressed normal to $(10\bar{1}0)$ did not display the fracture instability of the earlier suite. A key difference in the two suites of samples was that the first deformed by single slip $(2\bar{1}\,\bar{1}0)[0001]$ with well-developed slip arrays of dislocations whereas the second suite deformed by a fairly uniform distribution of dual slip on symmetrically equivalent systems $(01\bar{1}0)[2\bar{1}\,\bar{1}0]$ and $(1\bar{1}00)[11\bar{2}0]$ without prominent slip bands. This suggests that localization of stress or strain associated with slip bands plays a key role in the fracture instability.

Earlier studies of the fracture strength of synthetic quartz used a spherical indentor to establish the critical force required for growth of ring and cone fractures, beneath the indentor (Hartley & Wilshaw 1973, Swain *et al.* 1973). The latter study found a very sharp relative minimum in quartz inelastic strength near the α–β transition temperature (Fig. 4). It is especially significant that SiO_2 glass shows no such strength minimum in identical indentation fracture experiments, demonstrating that the crystalline quartz structure and α–β transition are essential factors in the fracture instability. Darot *et al.* (1985) also observed a similar strength reduction associated with the α–β transition in Vicker (diamond-pyramid) indentation hardness tests on quartz.

The α–β transition, being a displacive transformation, involves no bond breaking (e.g. Grimm & Dorner 1975). The essential co-ordinated atomic movements are characterized by systematic changes in the angle of tilt of $[SiO_4]^{4-}$ tetrahedra toward high-symmetry orientations. Using Landau theory, one can associate the degree of tetrahedral tilt with a thermodynamic order parameter and describe the systematic changes in quartz properties at temperatures approaching the α–β transition (Dolino 1988). Dauphiné twinning of α-quartz also involves systematic tilting of $[SiO_4]^{4-}$ tetrahedra, but to low-symmetry orientations that are symmetrically equivalent by the Dauphiné twin law. Transformation to β phase can be considered as Dauphiné twinning taken to the scale of the unit cell. Dauphiné twin structures consistent with this mechanism are observed in images from *in situ* high-temperature electron microscopy and in neutron diffraction experiments (Van Tendeloo *et al.* 1976, Dolino *et al.* 1984, Van Landuyt *et al.*1985, Snoeck *et al.* 1986). Domain structure consisting of fine-scale Dauphiné twinning near the α–β transition is, in fact, considered a transitional or incommensurate phase that forms first-order and second-order phase boundaries, respectively, with the α and β phases and is stable over an interval of about 2°C (Fig. 2b).

One possible interpretation of the α–β fracture instability observed in the experimental studies summarized above is that the incommensurate phase has a

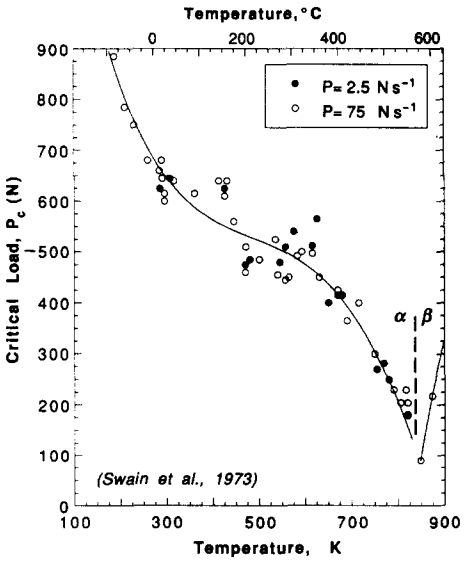

Fig. 4. Hertzian fracture strength of quartz under vacuum, after Swain *et al.* (1973). The inelastic strength of crystalline SiO_2 drops to nearly zero at $T = 573$ K, where α-quartz undergoes the displacive α–IC–β transformation, where IC is an incommensurate intermediate phase.

vanishingly-low fracture surface energy. This explanation in its simplest form, however, is inconsistent with the observation that fracture strength of α-quartz decreases systematically as temperatures *approach* the field of the incommensurate phase, not just at temperatures in the stability field of the incommensurate phase. The local stress state at the tip of a tensile crack could be sufficiently tensile (3–6 GPa) to depress $T_{\alpha-\beta}$ perhaps by as much as 300°C, however. The broad nature of the thermal fracture strength weakening may also be attributable to the unusually rapid decrease in elastic stiffness of α-quartz with increasing temperature (Darot *et al.* 1985), a property that decreases fracture surface energy and the work of fracture.

Another possible explanation of this anomalous brittle behavior is that the interatomic potential for α-quartz has a double minimum, with the minima at the order parameter associated with each Dauphiné twin state, similar to that postulated for other displacive transformations (Carpenter & Salje 1989). As the transition temperature is approached with increasing temperature, the minimum positions converge, resulting in a single, broad, elastically compliant minimum. This is consistent with the steeply increasing macroscopic elastic compliance of α-quartz with increasing temperature. A consequence of the broad minimum is that the expected amplitudes of thermal vibration should be larger, which could result in enhanced rates of thermally-activated processes involving Si–O bond breaking, such as fracture growth. However, the lack of evidence for an effect of loading rate on the critical load for Hertzian cone fractures (Fig. 4) argues against this explanation.

In order to gain insight into this instability in inelastic behavior, direct optical and TEM observation of growing crack tips in the vicinity of $T_{\alpha-\beta}$ are required. The large number of displacive transformations in rock-forming silicates and other minerals (Table 1) suggests that there is the potential for fracture instability to occur in many minerals other than quartz. Field observations of tectonites bearing these minerals and deformed near T_c might enable us to test this hypthosis in addition to laboratory experiments on these minerals. In particular, microfractures and healed microfractures may occur in minerals carried through such transformations while under stress. Quartz-bearing rocks in the thermal aureoles of mafic and intermediate crustal plutons, for example, might be settings to investigate. Vestigial Dauphiné twins produced by the α–β transformation near microfractures may be our best field record of interactions between microfracturing and transformation.

MARTENSITIC-LIKE TRANSFORMATIONS

Martensitic-like transformations are coherent transformations in which transformation strains are dominately shear rather than volumetric (see Heuer & Nord 1976, Porter & Easterling 1981 and Lorimer 1988 for reviews). By coherent, we mean that the host–martensite orientations and transformation strain are specified by the crystallography of the parent and martensitic phases, which are continuous across their interface or habit plane. The habit plane is typically undistorted (invariant) and the strain is described by a simple homogeneous shear γ parallel to it. The classic martensite is the phase that forms in austenitic carbon steels during rapid cooling. In metals, transformations of this type do not usually involve diffusion of mass species. Many martensitic phases occur in metals and they play important roles in alloy strengthening and exotic properties such as shape memory. Some martensites are considered polymorphs that have a low-temperature stability field but often do not form under slow cooling conditions because of kinetic hindrances to their nucleation and growth, such as the strain energy that accompanies martensite formation. Shear stress favors the formation of martensites because of the martensitic transformation shear strain (equation 2). Predictions of the effects of non-hydrostatic stress on martensite stability based on applications of equations (2) and (3) to uniaxial compression (Patel & Cohen 1953) are generally in good agreement with experimental data in many metallic systems (e.g. Friend & Miodownik 1988).

Martensitic-like transformations that occur in minerals are summarized in Table 2. In only two of these examples (würtzite–sphalerite and orthoenstatite–clinoenstatite) has the transformation strain actually been measured and shown to conform to the model of simple shear parallel to an invariant habit plane. Some martensitic-like phases have been observed as plate-like lamellae in deformed parent phases with the interphase contacts remaining essentially undistorted. In other polymorphic pairs, their crystallographic structures point to a possible relationship by shear deformation. These transformations are termed martensitic-like because they may involve short-range atom migration or 'shuffling' and bond breaking, processes atypical of martensitic transformations in metals, but similar to true martensites as they are coherent and have shear transformation strains larger than their volumetric strains. In some ways, transformations of this type in minerals are simpler than in metals because minerals have lower symmetry and hence there are fewer symmetrically-equivalent habit planes, typically only one.

Many of the mineral pairs in Table 2 are polytypes; i.e. related to one another by differences in stacking sequence. Simple shear on the stacking plane can transform the parent phase to the martensitic-like phase. A spectacular example of this occurs during the cooling of würtzite (stacking sequence ABABAB..., space group $P6_3mc$) grown from a ZnS vapor phase in the form of needles oriented normal to (0001) (Fig. 5). At temperatures below about 1027°C, the initially straight needles of würtzite transform partially to sphalerite (stacking, ABCABC..., space group $F\bar{4}3m$) and other polytypes, which results in the needles shearing by restacking and rotating their external crystal faces. The measured rotation angle of tilted sphalerite domains is about 19.3 ± 0.3°, close to the 19.47° angle predicted from crystallo-

Table 2. Martensitic-like transformations in rock-forming minerals

Formula	Parent Phase (space group)	Martensitic Phase	Orientation Relationships	Glide System	Shear Angle[§] Ψ, calc.	$\Delta V^*/V_o$	Transformation Partial Dislocation	References
ZnS	Würtzite (2H) *($P6_3mc$)*	Sphalerite (3C) *($F\bar{4}3m$)*	$(0001)_w = \{111\}_s$ $<1\bar{1}00>_w = [1\bar{1}0]_s$	{0001}<1$\bar{1}$00>	19.47° (19.4±0.3)	+0.001	b= 1/3<1$\bar{1}$00>	Mardix *et al.* (1968), Mardix & Steinberger (1970), Mardix (1986), D'Aragona *et al.* (1966), Akizuki (1981)
Mg_2SiO_4	(a) Olivine *($Pbnm$)*	Spinel, γ (Ringwoodite); *($Fd\bar{3}m$)*	$(100)_o=(111)_s$; $[001]_o=[1\bar{1}0]_s$; $[010]_o=[11\bar{2}]_s$	(100) [001]	19.9° 19.7°[(a)]	-0.085[1]	b= 1/12<013> b= 1/6[010][(a)]	Poirier (1981), Lacam *et al.* (1980); Hornstra (1960)
	(b) Spinel, γ *($Fd\bar{3}m$)*	β-phase *($Imma$)*	$[001]_\gamma=[001]_\beta$; $[110]_\gamma=[010]_\beta$	(110) [1$\bar{1}$2]	40.89°	+0.024[2]	b= 1/4[1$\bar{1}$2]	Price *et al.* (1982), Brearley *et al.* (1992), Madon & Poirier (1983)
Mg_2GeO_4	Olivine Germanate	Spinel, γ Germanate	$(100)_o=(111)_s$; $[001]_o=[\bar{1}10]_s$	(100) [001]	19.45° 19.3°[(a)]	-0.087[3]	b= 1/12<013> b= 1/6[010][(a)]	Burnley & Green (1989)
$MgSiO_3$	(a) Orthoenstatite *($Pbca$)*	Clinoenstatite low, *($P2_1/c$)*	$(100)_o=(100)_c$; $[001]_o=[001]_c$	(100) [001]	13.3° (12.8±1.3)	±0.001	b= 5/6[001]	Brown *et al.* (1961), Turner *et al.* (1960), Coe (1970), Coe & Kirby (1975)
	(b) Protoenstatite *($Pbcn$)*	Clinoenstatite *($P2_1/c$ or $C2/c$)*	$(100)_p=(100)_c$; $[001]_p=[001]_c$	(100) [001]	13.3° 11.9°*($C2/c$)*	±0.001[4]		Lee & Heuer (1987), Smyth (1974)
$Fe_{0.9}Mg_{0.1}SiO_3$	Orthoferrosilite *($Pbca$)*	Clinoferrosilite high, *($C2/c$)*	$(100)_o=(100)_c$; $[001]_o=[001]_c$	(100) [001]	13.3°	-0.003	b= 5/6[001]	Sueno *et al.* (1985), Coe (1970)
$CaSiO_3$	(a) Parawollastonite *($P2_1/a$)*	Wollastonite *($P\bar{1}$)*	$(100)_p=(100)_w$; $[010]_p=[010]_w$	(100) [010]	13.4°	±0.001	b= 1/2[010]	Trojer (1968), Coe (1970), Wenk (1969), Wenk *et al.* (1976)
	(b) Parawollastonite *($P2_1/a$)*	Bustamite *($I\bar{1}$)*	$(001)_p=(001)_b$; $[010]_p=[010]_b$	(001) [010]	13.7°	-0.060	b= 1/2[010]	Angel (1985)
Ca_2SiO_4	Ortholarnite, α'_L *($Ccm2_1$)*	Clinolarnite *($P112_1/n$)*	$(100)_o=(100)_c$; $[010]_o=[001]_c$	(100) [010]	4.5°	-0.035[5]		Kriven (1988)
$Ca_2Al_3Si_3O_{12}(OH)$	Zoisite *($Pnma$)*	Clinozoisite *($P2_1/m$)*	$(100)_z=(100)_c$; $[010]_z=[010]_c$	(100) [001]	8.8°	+0.038	b= 1/4[001]	Ray *et al.* (1986)
Al_2SiO_5	Sillimanite *($Pbnm$)*	Kyanite *($P\bar{1}$)*	$(010)_s=(010)_k$; $[001]_s\cong[001]_k$	(010) [100]	26.1°	-0.110	b= 1/2[100]	Doukhan & Christie (1982), Doukhan *et al.* (1985)
$Fe_2Al_4O_2[SiO_4]_2(OH)_4$	Chloritoid monocl. *($C2/c$)*	Chloritoid triclinic *($C\bar{1}$)*	$(001)_m=(001)_t$; $[100]_m=[100]_t$	(001) [010]	7.05°	-0.021		Hanscom (1975, 1980), Halferdahl (1961)
$(Al,Mg)_8(Al,Si)_6O_{20}$	Sapphirine monocl. *($P2_1/a$)*	Sapphirine tricl. *($P\bar{1}$)*	$(010)_m=(010)_t$; $[100]_m=[100]_t$	(010) [100]	21.4°	+0.028	b= 1/2[100]	Higgins *et al.* (1979), Christy & Putnis (1988)
TiO_2	(a) Anatase *($I4_1/m2/a2/d$)*	TiO_2 II *($Pbcn$)*	$(112)_a=(100)_{II}$; $[110]_a=[010]_{II}$	(112) [1$\bar{1}$0]		-0.048		Simons & Dachille (1970), Dandurand *et al.* (1982)
	(b) Rutile *($P4_2/m2_1/n2/m$)*	TiO_2 II *($Pbcn$)*	$(100)_r=(100)_{II}$; $[010]_r=[001]_{II}$	(100) [021]		-0.019		Simons & Dachille (1970)
$CaCO_3$	Calcite *($R\bar{3}2/c$)*	Aragonite *($P2_1/m2_1/c2_1/n$)*	$(0001)_c=(001)_a$; $[10\bar{1}0]_c=[010]_a$	(0001) [$\bar{1}$2$\bar{1}$0]		+0.060	b= 1/3<$\bar{1}$2$\bar{1}$0>	Gillet & Madon (1982), Dasgupta (1963)
ZrO_2	Baddeleyite tetrag. *($P4_2/nmc$)*	Baddeleyite monocl. *($P2_1/c$)*	$(100)_t=(100)_m$; $[001]_t=[010]_m$	(100) [001]	8.78°	+0.031[6]		Bansal & Heuer (1974), Kriven *et al.* (1981)

§ Shear angles (Ψ) listed in parentheses are experimentally determined; shear angles noted [(a)] are calculated from the alternative partial dislocation scheme.

* $\Delta V/V_o$ calculated at STP unless noted: [1] 16.1 GPa, 1500 K; [2] 16.4 GPa, 1500 K; [3] 0.5 GPa, 1200 K; [4] 0.1 MPa, 1373 K; [5] 950 K; [6] 1229 K.

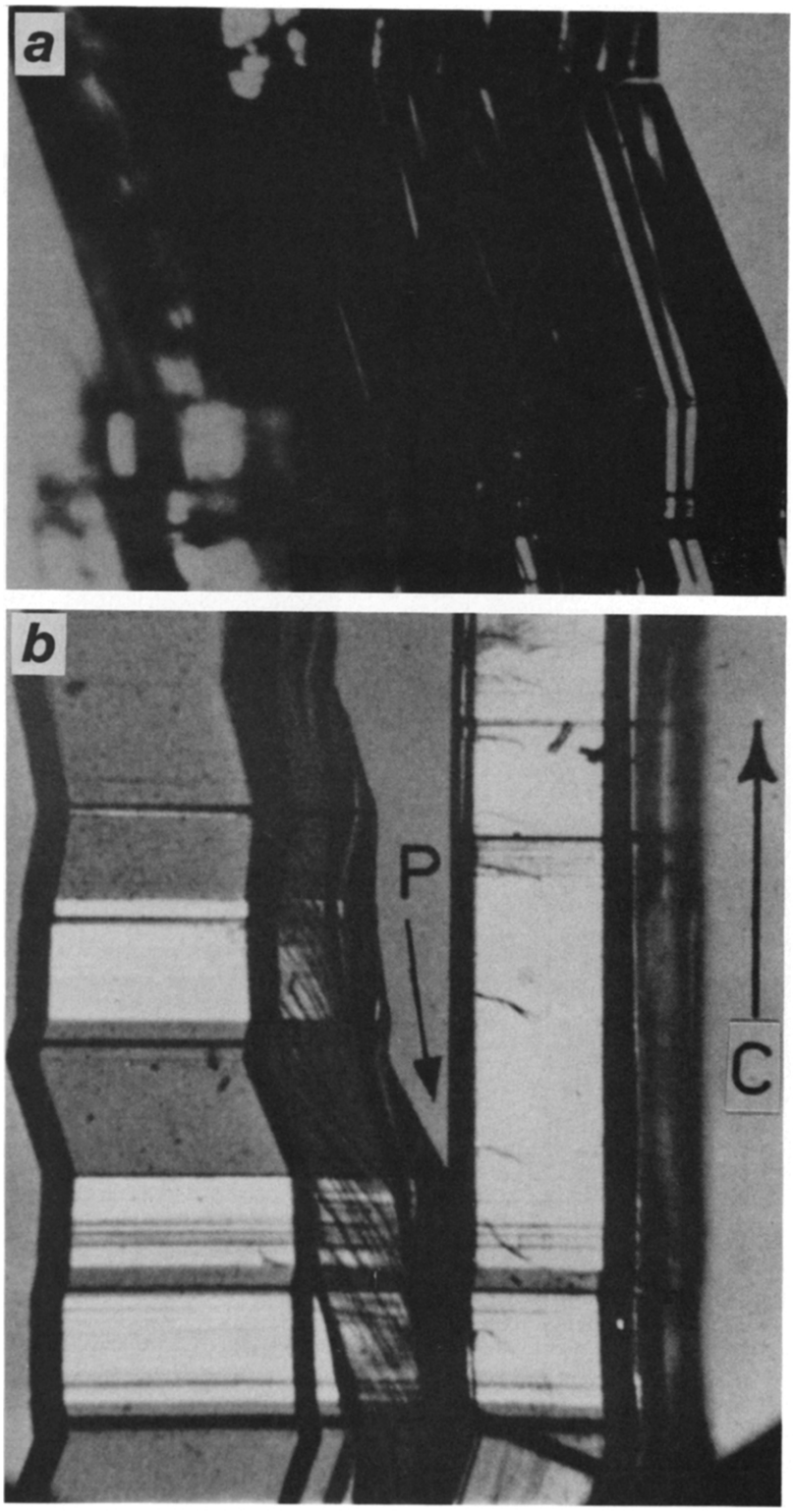

Fig. 5. (a) & (b) Micrographs (courtesy of S. Mardix) showing formation of martensitic-like sphalerite (ZnS) in initially straight needle-shaped würtzite single crystals. (a) Initially hexagonal 2H needles (würtzite) with parallel c axes partially transformed to sphalerite with an accompanying restacking and shear of 19.5°, tilting the needle facets. The vertical domains shown here remained hexagonal while the tilted domains became cubic (Mardix & Steinberger 1970). See text and Table 2. (b) Würtzite–sphalerite intergrowths in a cracked crystal, as viewed between crossed polarizing filters. Above point P, the two regions separated by a crack show different structure, the right side remaining würtzite and the left side transforming partially to sphalerite (darker domains that have tilted external boundaries) (Mardix *et al.* 1968).

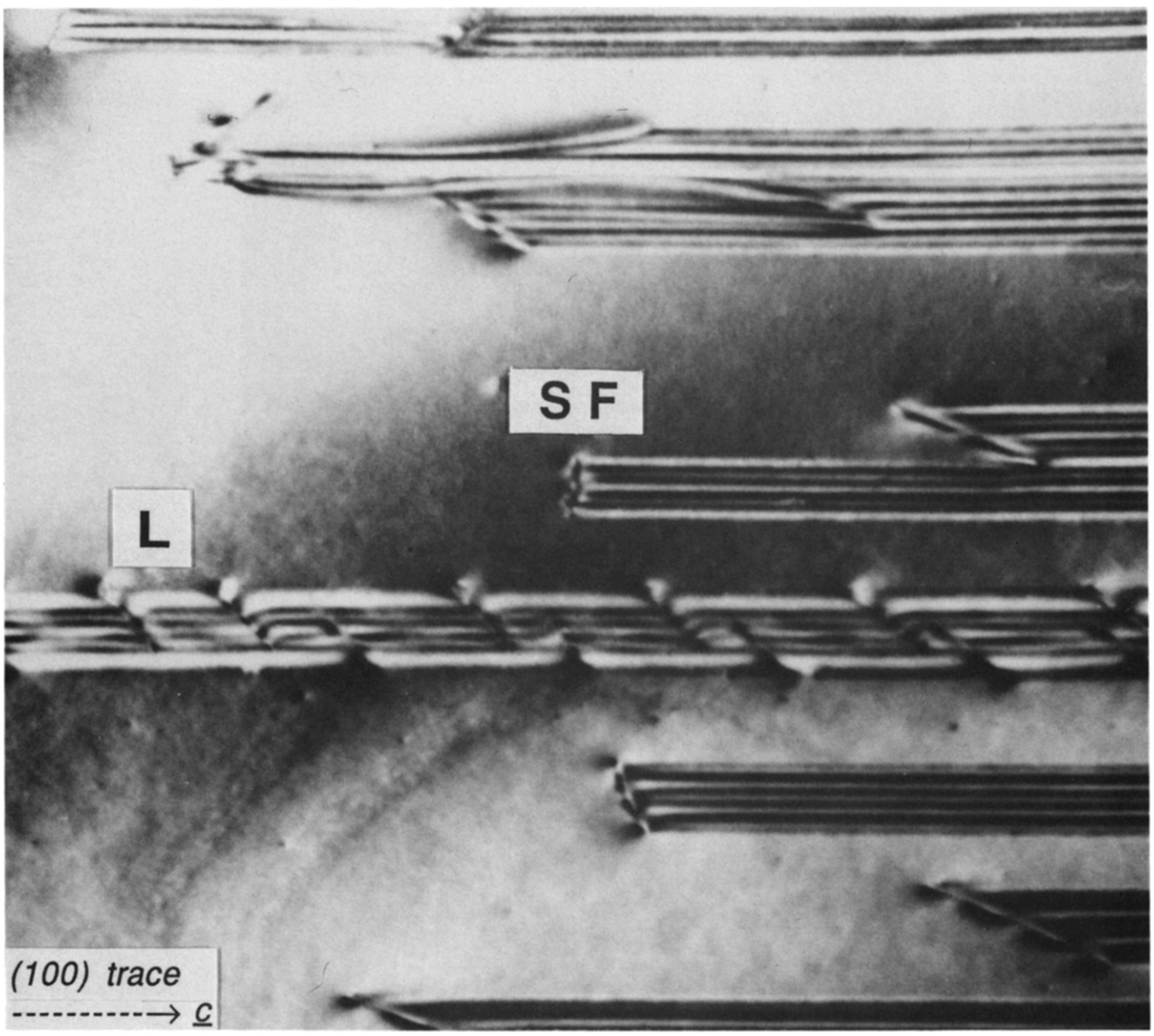

Fig. 6. Bright field TEM micrograph of orthoenstatite (OE) → clinoenstatite (CE) transformation showing lamellae of CE produced by experimental deformation of OE (Coe & Kirby 1975). **SF** is a stacking fault bounded by a $\mathbf{b} = 0.83[001]$ transformation partial dislocation, the motion of which transforms a double-wide OE cell to a two-unit cell wide slab of CE. **L** is a tapered lamella of CE with multiple transformation partial dislocations in its interphase boundaries (compare with Fig. 8).

graphic relations (Mardix *et al.* 1968, Mardix & Steinberger 1970, see also Akizuki 1981). A single screw dislocation often forms along the axis of the needles during growth (Mardix *et al.* 1987) and partial dislocations are nucleated from these growth dislocations. Spiral motion of these partials restacks the structure to the sphalerite polytype.

Martensitic-like transformations are potentially important under dynamic metamorphic conditions because shear stress τ resolved on the martensite plane and the direction of shear explicitly favors the martensitic-like phase and hence extends the phase's stability field to high temperature. Coe (1970) showed that for finite simple shear strain, the slope of the equilibrium line is given by

$$(d\tau/dT) = \Delta S/v_o\gamma, \quad (4)$$

where τ is the shear stress resolved in the martensite shear-strain co-ordinates and γ is the magnitude of the transformation simple shear strain, equal to the tangent of the angle of shear, Ψ (cf. equation 3). Measured and predicted values of Ψ are compiled in Table 2. To our knowledge, the predictions of equation (4) have not been quantitatively tested in any mineral system. It can also be shown that for a martensitic-like transformation, the P–τ slope of the equilibrium boundary is given by

$$dP/d\tau = \gamma/\varepsilon_v = \tan\Psi/\varepsilon_v. \quad (5)$$

Inspection of Table 2 for values of Ψ and $\varepsilon_v = \Delta V/V_o$ and calculation of $dP/d\tau$ from equation (5) show that in general shear stress should have a far larger effect on these equilibria than should pressure.

Although some of the martensitic-like mineral phases do form during cooling under macroscopically hydrostatic conditions in nature (such as (100) pigeonite in orthopyroxene host), others form only rarely during cooling. An example of the latter is low clinoenstatite (space group $p2_1/c$), a relatively rare monoclinic mafic mineral found only occasionally in volcanic rocks as a polysynthetically twinned phase or in deformed orthopyroxene-bearing rocks. Twinned low clinoenstatite (CE) may be synthesized readily in the laboratory by quenching orthorhombic protoenstatite (PE, space group *Pbcn*), from high temperatures. PE and orthoenstatite (OE, space group *Pbca*) both have double cell dimensions of 1.8 nm parallel to [100], where two 0.9 nm subcells of nearly CE structure are oriented with respect to each other like twins (Fig. 7). Transformation of either orthorhombic structure to CE may be considered an 'untwinning' process where two 0.9 nm layers of CE result from untwinning one orthorhombic cell (Brown *et al.* 1961). High-resolution electron microscopy shows that CE resulting from deformation always occurs as multiples of two unit cells, consistent with this model (Coe & Müller 1973). CE therefore can be produced by two equivalent senses of shear on the shear system (100)[001]. Each sense of shear produces an orientation of CE that differs only in the monoclinic [100] direction. An important point here is that a single sense of shear on the OE or PE → CE glide system produces a single [100]

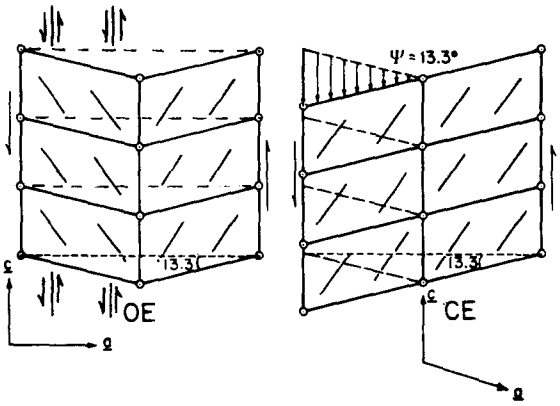

Fig. 7. Structural model for orthoenstatite → clinoenstatite transformation, after Coe & Kirby (1975). Clinoenstatite can be produced by either of two equivalent senses of shear on the shear system (100)[001], resulting in orientations of clinoenstatite that differ only in the monoclinic [100] direction.

orientation of CE, whereas under nominally hydrostatic conditions during quenching, both [100] CE orientations can and do occur, producing (100) twin intergrowths. In contrast, CE formed by deformation in the laboratory (Coe & Kirby 1975) and in kink bands in nature (Trommsdorff & Wenk 1968, Coe & Müller 1973) is not twinned. This difference may serve to distinguish martensitic-like phases formed by cooling from those formed through the assistance of nonhydrostatic stress.

The experiments cited by Coe & Kirby (1975) indicate that CE has a true low-temperature stability field with a zero-pressure intercept of the equilibrium line with orthoenstatite (*Pbca*), OE, at about 566°C and a pressure derivative of 45°C GPa^{-1}. In striking contrast, CE is readily produced from OE at temperatures as high as 1300°C under shear stress in deformation experiments (Coe & Kirby 1975). Predictions from equation (4) of the effect of shear stress τ on the extension of clinoenstatite stability cluster around 3000°C GPa^{-1}, almost 70 times the effect of pressure. These predictions are consistent with the formation of clinoenstatite in deformation experiments at temperatures far higher than 566°C when τ was as high as 0.25 GPa.

Coe & Kirby (1975) and McLaren & Etheridge (1976) have shown by TEM that the micromechanism of CE formation from OE under stress involves the nucleation of partial dislocations from pre-existing unit dislocations (with Burgers vector $\mathbf{b}$ = [001]) by the dissociation reaction [001] → 0.17[001] + 0.83[001]. The subsequent glide of each mobile $\mathbf{b}$ = 0.83[001] transformation partial dislocation in the (100) plane produces lamellae of CE two unit cells thick (Fig. 6, SF), a prediction borne out by direct counts of partials and the thickening of CE lamellae in OE (Fig. 6, L). The OE → CE transformation therefore is a type of plasticity, like intracrystalline slip and mechanical twinning, that involves the nucleation and migration of crystal dislocations under shear stress.

Stress-assisted martensitic-like polymorphs are likely to be important in nature for several reasons: (1) they provide a micromechanism for inelastic deformation and can affect rock rheology; (2) their presence or

absence may be diagnostic of the prior thermodynamic state of the system, particularly the stress state (Coe & Kirby 1975); and (3) the relatively rapid kinetics associated with co-operative atom motions under stress may make nucleation and growth easy (Poirier 1981), like the similar process of mechanical twinning (e.g. Kirby & Christie 1977). Martensitic-like transformations may therefore contribute to metamorphic processes that occur in fast strain rate environments, such as in meteorite impacts and seismic fault zones. More studies are needed on metamorphic tectonites that bear these phases in order to test these ideas. In particular, lamellar intergrowth structures parallel to the expected invariant or contact planes (Table 2) should be investigated at optical and TEM scales. Cation site occupancies may also be altered by martensitic-like transformations, as suggested, for example, by the structural model of Coe & Kirby (1975) for orthoenstatite → clinoenstatite.

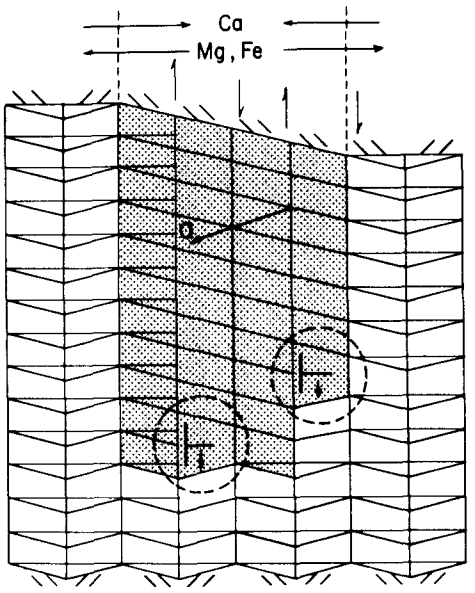

Fig. 8. Structural model for the exsolution of *C*2/*c* Ca-clinopyroxene that is thought to occur by orthopyroxene → clinopyroxene transformation shear (Fig. 7) and cation exchange, after Kirby & Etheridge (1981). Passage of **b** = 0.83[001] partial dislocations (recumbent 'T' symbols) produces lamellae (shaded) of monoclinic pyroxene with *a*-axis orientation as shown, and cation exchange (indicated at top) produces calcic clinopyroxene. Slashes at top and bottom indicate axis orientation of Mg–Fe co-ordination octahedra most nearly parallel to (010). Continued passage of partial dislocations into adjacent orthopyroxene cell leads to growth at ledges on the interface and thickening of exsolution lamella.

COHERENT EXSOLUTION AND PRECIPITATION

Minerals show an astonishing variety of intergrowths associated with exsolution during cooling. Under hydrostatic conditions, most, if not all, of these transformations are driven by changes in the entropy of mixing during cooling. However, among those that have coherency or structural continuity between host and exsolved phases, some require restacking of the structure that involves very large shear strains. This fact points to shear stress as an intensive variable affecting the stability and kinetics of exsolution of these mineral species. A prime example is the exsolution of *C*2/*c* Ca-clinopyroxene from orthoenstatite (Kirby & Etheridge 1981). *C*2/*c* Ca-clinopyroxene is a stacking polytype that is identical to $P2_1/c$ clinoenstatite and different from the orthopyroxene host, requiring that coherent exsolution of Ca-clinopyroxene must involve at least local shear strain of $\gamma \approx \tan(13.3°) = 0.236$. Kirby & Etheridge (1981) proposed that this exsolution can therefore be considered to have two components (Fig. 8): (1) restacking of the structure by a shear identical to the OE → CE transformation described in the section above (Fig. 7); and (2) interdiffusion of Ca and (Mg,Fe). If this is correct, then Ca-clinopyroxene should have a preferred direction of [100] with respect to the sense of shear. They examined the [100] orientations of Ca-clinopyroxene exsolution lamellae in kinked OE, and found that the [100] orientations of the great majority of these lamellae in kinks conformed to that predicted from the OE → CE model shown in Figs. 7 and 8. In optically undeformed examples of OE in layered mafic complexes, the [100] orientations of the lamellae show an essentially random distribution of [100] axes on either side of the (100) plane, confirming observations by others (cited in Kirby & Etheridge 1981) and supporting the argument that differences in the level and spatial coherence of shear stress during lamellar growth played important roles in their development. TEM studies of (100) augite lamellae in orthoenstatite confirm the presence of ledge structures and elastic distortion consistent with transformation partial dislocations moving in the augite–orthoenstatite interface and restacking the orthoenstatite structure (Champness & Lorimer 1974, Kohlstedt & Vander Sande 1974, Kirby 1975 unpublished TEM investigation of Bamble (Norway) enstatite, Ross & Huebner 1979). Similar structural relations are found in the coherent exsolution of *C*2/*m* hornblende from *Pnma* orthoamphiboles (Smelik & Veblen 1992), suggesting that deformation may play a direct role in their formation similar to that found for exsolution in orthopyroxene. TEM investigations of coherent exsolution lamellae often report dislocations in the interphase boundaries and these are typically interpreted as misfit dislocations reflecting differences in cell parameters in the contact plane. Alternatively, these may represent partial dislocations responsible for restacking the structure and hence deformation should play an important role in their formation and migration.

The interdiffusion rates associated with exsolution in silicates are so slow that exsolution has been difficult to study experimentally (Buseck *et al.* 1980, Liu & Yund 1992). Good model systems for silicates are the binary oxide spinel structures because diffusion rates are relatively high at modest temperatures. Coherent exsolution has been studied under non-hydrostatic stress in two spinel bulk compositions: the mineral spinel, $MgO \cdot nAl_2O_3$, and nickel ferrite, $NiO \cdot nFe_2O_3$. In a remarkable study, Duclos (1979) demonstrated a stress-enhanced exsolution of corundum ($R\bar{3}c$) from

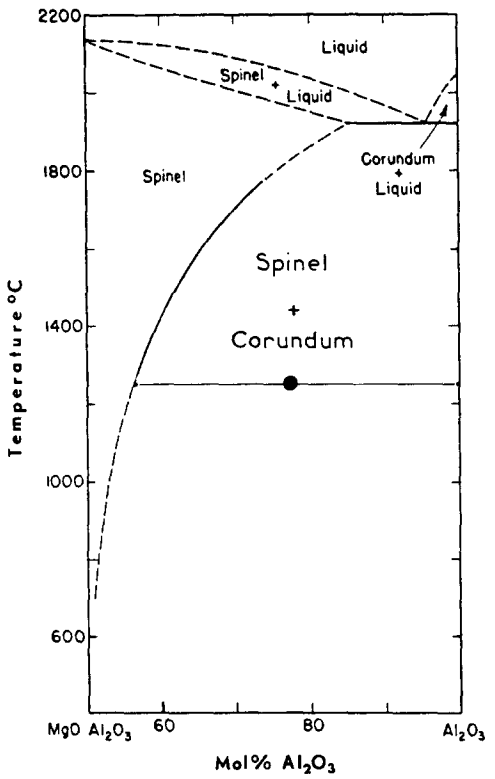

Fig. 9. Room-pressure MgO–Al_2O_3 phase diagram, after Roy *et al.* (1953) with conditions of precipitation experiments by Duclos (1979) designated by solid circle. The end points of the horizontal tie-line represent the equilibrium compositions of the spinel host and corundum precipitates.

$MgO \cdot 3.5Al_2O_3$ spinel grown to that metastable composition by the flame-fusion method. The reaction

$$MgO \cdot 3.5Al_2O_3 \text{ (metastable)} \rightarrow MgO \cdot 1.2Al_2O_3 + 2.3\,Al_2O_3$$

produced a spinel host composition consistent with the equilibrium solvus (Fig. 9). The creep tests were conducted under a uniaxial stress of 160 MPa and a temperature of 1220°C; shortening strains of 0.025–0.045 were sustained by the crystals at rates that were markedly higher than those of spinel equilibrium composition n = 1.1–1.2 (Fig. 10). The compression axis was oriented crystallographically in three directions: [001], [110] and [111]. Coherent corundum precipitates formed with (0001) parallel to the spinel (111) planes, in the first two cases parallel to the four and two (111) planes, respectively, that had the highest resolved shear stress on the glide system $\{111\}\langle 11\bar{2}\rangle$. For the case of the third compression direction, a single set of corundum precipitates grew perpendicular to the shortening direction and parallel to the {111} plane in the host spinel. Coherent corundum precipitation preserves the oxygen close-packed plane but the FCC → HCP restacking requires a macroscopic shear of 19.47° between the oxygen close-packed layers in $\langle 11\bar{2}\rangle$ directions, like the restacking of sulfur atoms in the würtzite → sphalerite transformation described above. Interdiffusion of Mg and Al evidently completes the precipitation process.

The detailed role of applied deviatoric stress in corundum precipitation is not established. However, the fact

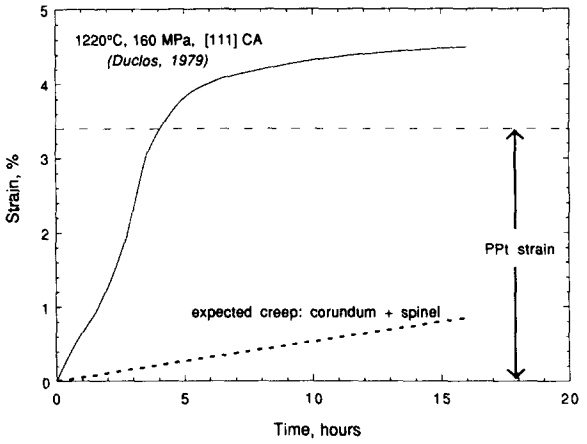

Fig. 10. Creep curve during α-Al_2O_3 precipitation from a single crystal $MgO \cdot 3.5Al_2O_3$ matrix, after Duclos (1979), obtained in air at 1220°C with 160 MPa stress directed along the [111] compression axis (CA). Below a strain of approximately ε = 3.4%, the accelerated strain induced by Al_2O_3 precipitation (designated PPt strain) produces the steeply-rising lower portion of the S-shaped curve, whereas above ε = 3.4% (post-precipitation), the rate slows to values of order 10^{-8} s^{-1}, comparable to the expected creep rate of corundum + spinel (dashed line).

that those (111) precipitates formed in the first two compression directions were on the planes that had the highest resolved shear stress for oxygen restacking suggests that shear stress played an important role in the required restacking, confirming earlier results by Veyssière (1977) on the precipitation of hematite ($R\bar{3}c$) from nickel ferrite.

Compressive stress perpendicular to the close-packed plane, i.e. in the [111] direction, also facilitates corundum precipitation because the resultant interlayered spinel–corundum is 3.4% more compact in that direction than the original spinel (Fig. 11). The rate of corundum precipitation under these conditions was fas-

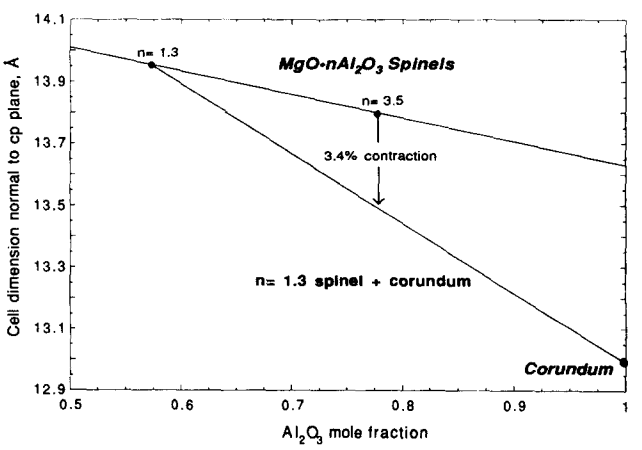

Fig. 11. Cell dimension changes perpendicular to the close-packed (cp) plane accompanying exsolution of $MgO \cdot nAl_2O_3$ spinels. Precipitation of the denser alumina phase from the matrix effectively reduces the total sample volume, and for the exsolution reaction $MgO \cdot 3.5Al_2O_3 \rightarrow 2.2Al_2O_3 + MgO \cdot 1.3Al_2O_3$ the cell dimension of the resultant interlayered phases measured in the cp plane results in a 3.4% contraction. This is in close agreement with the compression strain produced in Fig. 10, and shows that compressive stress normal to the cp plane facilitates corundum precipitation and produces a significantly higher initial transient rate of shortening associated with precipitation.

ter than the rate of plastic deformation by dislocation creep and hence a markedly higher initial transient rate of shortening associated with precipitation occurred prior to an approach to steady state (Fig. 10). Comparison with the steady-state rate of dislocation creep of mixed equilibrium spinel and corundum indicates an anomalous creep strain of about 3.5%, essentially identical to the predicted precipitation shortening.

Anomalous transient creep also occurred in the n = 3.5 spinel compressed in the [100] and [110] directions, but at rates and total transient strains less than those in the [111] direction (Duclos 1979). For reasons not understood, compressive stress normal to the plane of precipitation is more effective in promoting corundum exsolution than is shear stress, even though the driving potential for exsolution is more than twice as high in the two high shear stress orientations.

To our knowledge, there has not been a comparable experimental study of exsolution under deviatoric stress in another rock-forming mineral. Although much work has been done on the misfit strains between interfaces along precipitation intergrowths in silicate solid solutions (the coherent spinodal: e.g. Robin 1974, Yund & Tullis 1983a,b), there has been no investigation into the effects of restacking and interface-normal contraction on precipitation under deviatoric stress. One of the possible ways of detecting effects of non-hydrostatic stresses on coherent exsolution is that in many exsolution pairs, such as orthoenstatite–augite, a specific crystallographic orientation of the exsolved phase is associated with a given sense of shear, whereas in the absence of a uniform non-hydrostatic stress, there are additional degrees of freedom in the orientation of the exsolved phase (e.g. Kirby & Etheridge 1981).

ORDER–DISORDER TRANSFORMATIONS

Cation site occupancies are to varying degrees disordered at high temperatures and ordered at low temperatures. An order–disorder transformation under stress has been implicated in the anomalous plastic yield strengthening with increasing temperature of $MgO \cdot nAl_2O_3$ spinels of composition n = 1.1. That composition is close to equilibrium along the solvus in the MgO–Al_2O_3 system at T = 400–1000°C (Fig. 9) and consequently the mechanical effects of exsolution–precipitation described in the previous section are not expected. The crystals were grown by very slowly pulling a rotating seed crystal from the melt. Initial investigation of plastic deformation at 400°C and a confining pressure of 1.4 GPa indicated that easy glide occurs on the slip system $\{110\}\langle 1\bar{1}0\rangle$ (Kirby & Veyssière 1980). Subsequent experiments (Veyssière *et al.* 1980), however, revealed something totally unexpected: the spinel crystals deforming by this slip system became stronger, not weaker, with increasing temperature between 500 and 950°C (Fig. 12a). This result was in marked contrast with the weakening behavior of most crystalline materials that generally follow the same rate laws as most ther-

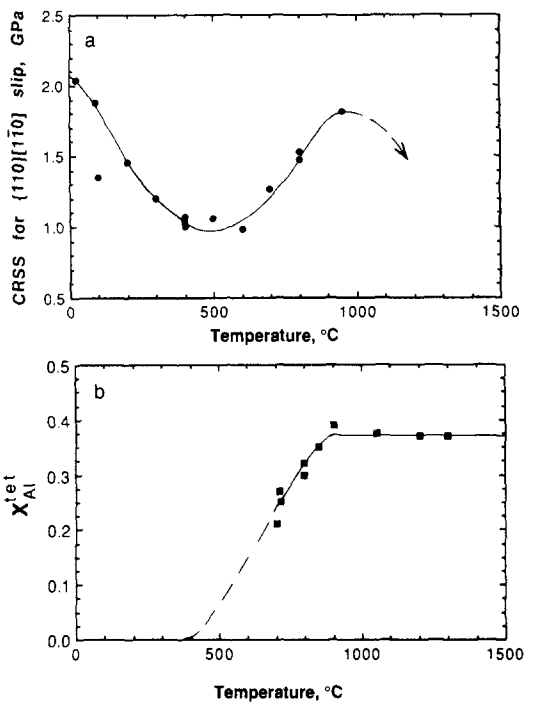

Fig. 12. (a) Variation of the critical resolved shear stress, CRSS, for $\{110\}\langle 1\bar{1}0\rangle$ slip in spinel at 1.4 GPa confining pressure, from Kirby & Veyssière (1980) and Veyssière *et al.* (1980). Spinel crystals deforming by glide along the $\{110\}\langle 1\bar{1}0\rangle$ slip system show anomalous strengthening within the 500–900°C temperature interval. (b) Temperature effect on proportion of Al atoms in tetrahedral sites shows that spinel undergoes an order–disorder transition over approximately the same temperature interval in which strengthening occurs (Wood *et al.* 1986).

mally activated processes. Neither of the end members of the binary MgO–Al_2O_3 system, corundum (Al_2O_3) and periclase (MgO), display such an anomalous strengthening effect over the same temperature interval (Paterson & Weaver 1970, Castaing *et al.* 1981). Moreover, spinel at very high temperature weakens with increasing temperature (Duclos *et al.* 1978).

What causes spinel to strengthen with increasing temperature over this interval? Subsequent measurements of the proportion of Al atoms in tetrahedral sites indicated that spinel undergoes an order–disorder transformation in the temperature interval 500–900°C, approximately the same temperature interval in which the anomalous strengthening occurs (Fig. 12b). The disordering transformation is:

$$Mg^{IV}Al_2{}^{VI}O_4 \rightarrow (1-x)\,Mg^{IV}Al_2{}^{VI}O_4 + x\,[Al^{IV}(Mg + Al^{VI})O_4],$$

where the Roman numerals indicate the cation co-ordination state with oxygen and x is the mole fraction of aluminum in tetrahedral co-ordination. Aluminum siting is disordered as a mix of octahedral (VI) and tetrahedral (IV) positions. The very slow cooling of these crystals during growth would suggest that the starting materials had Al mostly in VI-fold co-ordination.

The correlation between the anomalous and striking effect of temperature on plastic yield strength and the aluminum disordering reaction over the same temperature interval suggests that the two phenomena are re-

lated. Increases in plastic yield strength with temperature have been observed in a few types of crystalline compounds such as $L1_2$ metal alloys (binary or ternary superlattice alloys based on the close-packed fcc structure) and the mineral dolomite $CaMg(CO_3)_2$ (Barber *et al.* 1981). These compounds also show some degree of increasing positional disorder with increasing temperature. In oxides, dislocation motion in complex crystalline materials such as these often involves synchronized motion of cations in addition to those associated with the shear of the oxygens. These motions essentially restore the preferred cation co-ordination after shear has taken place on the glide plane (Kronberg 1957, Hornstra 1960). Termed synchroshear, the effects of these co-ordinated cation motions are thought in part to explain why close-packed oxides of various cation chemistries exhibit such a large range of plastic yield strengths. If cation positions are ordered, then their motion may in some instances be synchronized more easily to restore the preferred co-ordination. Veyssière & Carter (1988) demonstrated that dislocations in the same spinel samples deformed by Kirby & Veyssière (1980) and Veyssière *et al.* (1980) are typically split (dissociated) into partial dislocations by climb motion out of the slip plane and that samples deformed at 800–950°C have dislocation separations nearly ten times that of samples deformed at 400°C. They also presented evidence that the slip occurs by the co-ordinated motion of these partial dislocations and cation shuffles at the stacking fault in between. This suggests to us that cation disorder at the higher temperatures is playing an unknown role in decreasing the mobility of slip dislocations during glide. However, climb dissociation and temperature strengthening are not unique to systems that display order–disorder (Veyssière 1988).

The hypothesis that cation disorder can reduce dislocation mobility needs to be tested with specific positional models of dislocations in ordered and disordered states. Order–disorder reactions are extremely common in mineral systems and these experimental results suggest that mechanical effects of order–disorder reactions may be important in mineral rheology during changes in thermal regime and attendant site cation order.

NEAR-SURFACE DEVOLATILIZATION OF HYDROUS SILICATES

At temperatures well below nominal macroscopic dehydration temperatures, devolatilization of hydrous silicate single crystals can effectively produce anomalously brittle behavior in association with liberation of free water near microcracks. This phenomenon was unexpectedly discovered when Lee & Kirby (1984) conducted a suite of deformation experiments on single crystals of gem-quality topaz, $Al_2SiO_4(OH,F)_2$. Their goal was to establish the plastic deformation mechanisms of that mineral. The experiments were done at temperatures up to 950°C and a confining pressure of 1.5 GPa. Those conditions are normally adequate to suppress ordinary brittle fracture and permit plastic deformation in virtually all nominally-dry silicates, oxide ceramics and carbides (see references in Kirby *et al.* 1990). That study of topaz plasticity was a complete failure. No significant plastic deformation occurred in the variety of orientations of compression directions with respect to the perfect (100) cleavage. Subsequent experiments (Kirby *et al.* 1990) at 800°C and 1.5 GPa on a suite of single crystals of other hydrous minerals (epidote, tourmaline and tremolite) gave the same result: catastrophic failure by brittle fracture at stresses of 1–2.5 GPa (Fig. 13). The only other hydrous silicates that have shown significant plastic deformation under these conditions are the micas, such as biotite (Kronenberg *et al.* 1990) and muscovite (Mares & Kronenberg 1993). Micas are unusually weak in orientations with high shear stress on the basal plane because of weak bonding in the (001) interlayer containing the alkali ions. This role of the alkali interlayer in the low plastic yield strength of mica was confirmed by experiments in which mica crystals were compressed normal to the basal plane, an orientation that suppresses slip on the (001) plane; failure occurred by brittle fracture at stresses comparable to those measured in other hydrous minerals (Kronenberg *et al.* 1990, Mares & Kronenberg 1993). A second exception is plastic deformation of clinoamphiboles (space group $C2/m$) that mechanically twin at comparable temperatures in certain orientations of the direction of compression.

In short, hydrous minerals are fundamentally brittle. Why? Lee & Kirby (1984) suggested that structural water in hydrous silicates is somehow effective in migrating to nucleating cracks. They argued that this increases the rates of crack growth in ways similar to those by which molecular water in the environment of glasses, oxides and minerals increases the rates of crack growth by a process of chemical attack resulting from hydrolysis of stressed bonds at crack tips. No convincing independent evidence for migration of water to fracture surfaces was offered.

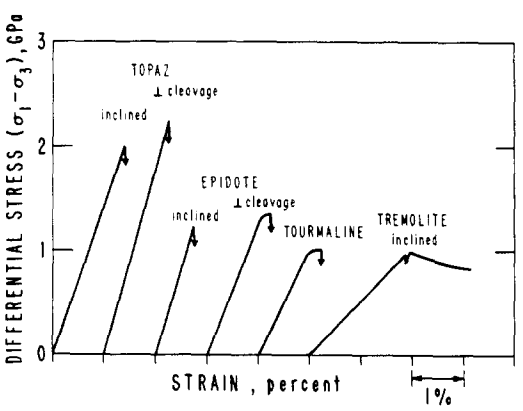

Fig. 13. Stress–strain curves (with staggered strain intercepts) of topaz, epidote, tourmaline and tremolite at 800°C, 1.5 GPa confining pressure and 2×10^{-5} s^{-1} strain rate, showing failure by brittle fracture at various orientations of compression with respect to (100) cleavage (after Lee & Kirby 1984, Kirby *et al.* 1990). That no significant plastic deformation occurred in any of the tests is indicative of the fundamental brittleness displayed by many hydrous minerals.

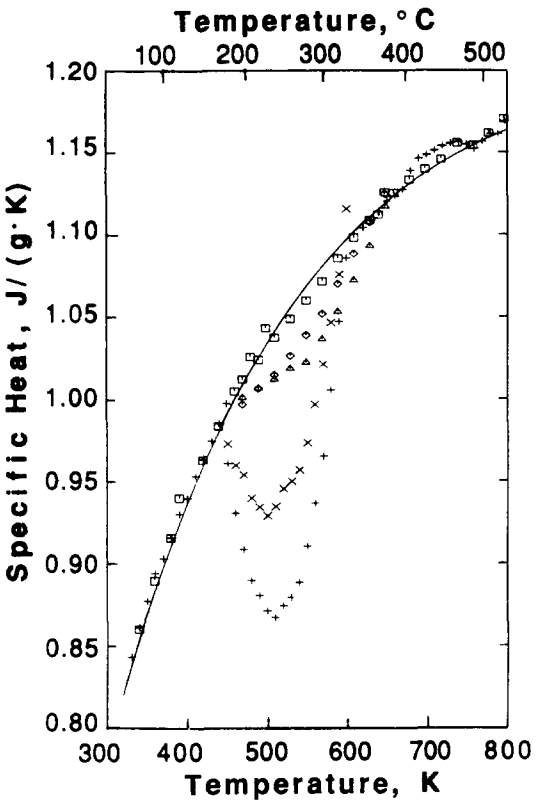

Fig. 14. Differential scanning calorimetry (dsc) scans from Kirby *et al.* (1990) show the thermal instability of powdered topaz. Measurements on large single-crystal topaz (squares) show monotonically increasing apparent heat capacity, C_p, with increasing temperature. No hysteresis was detected during heating and cooling cycles up to 527°C. Sieved powders of the same materials show the same behavior up to 177°C, above which prominent drops in apparent C_p occur. Decreasing powder grain size increases the downward deflection of C_p and increases the loss of total structural water, as detected by weight loss (see table 2 in Kirby *et al.* 1990).

Independently, B.S. Hemingway (unpublished data) found evidence for migration of water to fracture surfaces in the course of a systematic measurement program of heat capacities of hydrous minerals using the dsc technique (*d*ifferential *s*canning *c*alorimetry). Briefly, dsc measures the differential electrical power dissipated as heat required to maintain a sample and a reference material at the same temperature during a controlled constant rate of increase in temperature (a scan). A dry gas flowing through the chamber maintains an inert environment. The apparent heat capacity C_p may be calculated from the differential power curves vs time when suitable corrections are made. Large single crystals of hydrous minerals show monotonically increasing C_p typical of materials not undergoing changes of state (Fig. 14) and weight losses during temperature cycling are negligible. Also, no hysteresis is observed in heating and cooling cycles up to 527°C. Sieved powders of the same minerals show the same behavior up to 177°C, above which prominent drops in apparent C_p occur, indicating an energy absorbing process is occurring up to temperatures of 377°C. No anomaly in apparent C_p occurs during subsequent scans provided the sample environment is maintained dry. The finer the grain size of the powder, the bigger the downward deflection of the apparent C_p curve and the larger the weight loss that occurs during temperature cycling. Weight losses up to about 10% of the total structural water content (1.6–3.0%) were measured, and subsequent exposure to laboratory humidity partially restored the anomalous behavior in later dsc scans.

Kirby *et al.* (1990) interpreted these dsc findings as indicating that hydrogen near fracture surfaces is mobile and migrates to react with surface oxygens, and is then liberated from the surface as water vapor. They showed that this model of hydrogen migration is roughly consistent with measured values of intracrystalline hydrogen diffusion rates in silicates. Hydrogen in the ideal bulk crystal structures of hydrous minerals is essential for satisfying bonding requirements, and loss of protons, for example, would probably produce impossibly large space charges and consequent gradients in electrical potential. Surfaces of silicates, however, may have substantially different structures in which the structural roles of hydrogen may be quite different. The fact that smaller grain sizes and hence larger fracture surface areas increase the magnitudes of the dsc anomalies points to a critical role of fracture surfaces in this thermal instability of powdered hydrous minerals. That water is liberated is demonstrated by the weight-loss measurements and by the partial restoration of anomalous dsc behavior and weight gain by subsequent exposure to humid air. The availability of water from fracture surfaces inside hydrous mineral crystals should facilitate crack growth in ways similar to that of water in the environment of nominally anhydrous silicates under stress (e.g. Wiederhorn 1978, Atkinson & Meredith 1981, Michalske & Freiman 1983).

The fracture stresses shown in Fig. 13 are probably too high to occur in the Earth's crust. However, longer time scales of deformation at lower strain rates in nature and lower normal stresses and pressures than shown in Fig. 13 may substantially reduce fracture strengths of these minerals. We obviously need better characterization of hydrous silicate surface structures to improve our knowledge of how water interacts with them. Structural petrologists studying naturally deformed rocks that bear hydrous minerals should be aware of the potential of intracrystalline water in embrittlement even under conditions in which the bulk hydrated phase may be thermally stable. Microscopic evidence for devolatilization near microfractures might be found in naturally-deformed rocks as microfractures localized in hydrous minerals. There is an important distinction between the phenomenon we have just described and the well known bulk dehydration embrittlement of hydrous silicates originally discovered by Raleigh & Paterson (1965) and attributed by them primarily to the effects of pore fluid pressure in reducing effective pressures.

SUMMARY AND CONCLUSIONS

Mineral single crystals display an impressive range of anomalous mechanical behavior as they undergo changes of state under stress. In the examples cited, the

transformations are of the simplest kind such that the initial crystal structure is only partially changed during transformation. Some of these changes in mineralogy involve minor changes in the articulation of the cation co-ordination polyhedra, others involve shear of a layered structure, and in others cation diffusion must also take place. Anomalous mechanical response to applied stresses ranges from embrittlement to enhanced rates of plastic deformation to plastic strengthening with increasing temperatures.

While we have restricted the present paper to a review of metamorphic processes that occur primarily in grain interiors, most of the important phase changes that occur during metamorphism evidently involve wholesale changes in crystal structure that occur at ordinary interphase grain boundaries. We have only begun to explore reconstructive phase changes of the simplest congruent type where no chemical exchange occurs, and even in these polymorphic transformations the variety of mechanical response to applied stresses is remarkable. For example, there is a remarkable range of grain textures produced during reconstructive polymorphic phase changes in ice I → II (Kirby *et al.* 1991, 1992), Mg_2GeO_4 and $(Mg,Fe)_2SiO_4$ olivine → spinel (Green & Burnley 1989, Green *et al.* 1990, Burnley *et al.* 1991, Tingle *et al.* 1993) and calcite → aragonite (Hacker & Kirby 1993). Some of the observed textures resemble those found in metamorphic rocks. The inelastic responses of these mineral systems during transformation under stress range from macroscopically uniform ductile deformation with or without strain softening, to a new type of high-pressure faulting termed *transformational faulting* (see reviews in Kirby 1987, Green & Burnley, 1989, Burnley *et al.* 1991, Kirby *et al.* 1991, 1992). Assessment of the marked effects which localized reconstructive phase transformations can have on the character of inelastic deformation is beyond the scope of this review. The discovery of transformational faulting in both H_2O ice and olivine germanate provides a case in point; unlike faulting by ordinary brittle fracture, transformational faults form at stresses that are insensitive to variations in normal stress and pressure. This property makes the mechanism of transformational faulting an attractive candidate for faulting and earthquakes in deeply subducted lithosphere where mantle phase changes are taking place (Kirby 1987, Green *et al.* 1990, Kirby *et al.* 1991).

Whether or not such anomalous mechanical responses to applied stress actually occur in the Earth needs to be tested by closely examining microstructures recorded in deformed rocks. Careful optical and TEM study of natural examples of minerals that have undergone changes of state are called for in order to establish whether or not microstructures characteristic of the processes outlined above have been produced during natural deformation.

Acknowledgements—S. H. Kirby gratefully recognizes the roles that John Christie has played in his development as a scientist and wishes him well on the occasion of his 60th birthday.

The authors thank Brad Hacker, Gordon Nord, Bruce Hemingway, Jan Tullis, Pamela Burnley and Jean-Paul Poirier for their help in improving this paper. SHK also thanks Lisa Dell'Angelo for her help in searching the mineralogical literature.

REFERENCES

Akizuki, M. 1981. Investigation of phase transitions of natural ZnS minerals by high resolution electron microscopy. *Am. Miner.* **66**, 1006–1012.

Angel, R. J. 1985. Structural variation in wollastonite and bustamite. *Mineralog. Mag.* **49**, 37–48.

Angel, R. J. 1988. High-pressure structure of anorthite. *Am. Miner.* **73**, 1114–1119.

Atkinson, B. K. & Meredith, P. G. 1981. Stress corrosion cracking of quartz: a note on the influence of chemical environment. *Tectonophysics* **77**, T1–T11.

Bansal, G. K. & Heuer, A. H. 1974. On a martensitic phase transformation in zirconia ZrO_2—II crystallographic aspects. *Acta metall.* **22**, 409–417.

Barber, D. J., Heard, H. C. & Wenk, H.-R. 1981. Deformation of dolomite single crystals from 20 to 800°C. *Phys. Chem. Miner.* **7**, 271–286.

Beach, A. 1980. Retrogressive metamorphic processes in shear zones with special reference to the Lewisian complex. *J. Struct. Geol.* **2**, 257–263.

Brearley, A. J., Rubie, D. C. & Ito, E. 1992. Mechanisms of the transformations between the α, β, and γ polymorphs of Mg_2SiO_4 at 15 GPa. *Phys. Chem. Miner.* **18**, 343–358.

Brodie, K. H. & Rutter, E. H. 1986. On the relationship between deformation and metamorphism, with special reference to the behavior of basic rocks. In: *Metamorphic Reactions* (edited by Thompson, A. & Rubie, D.). Springer, New York, 138–179.

Brodie, K. H. & Rutter, E. H. 1987. The role of transiently fine-grained reaction products in syntectonic metamorphism: natural and experimental examples. *Can. J. Earth Sci.* **24**, 556–564.

Brown, W. L., Morimoto, N. & Smith J. V. 1961. A structural explanation of the polymorphism and transitions of $MgSiO_3$. *J. Geol.* **69**, 609–616.

Burnley, P. & Green, H. 1989. Stress dependence of the mechanism of the olivine-spinel transformation. *Nature* **338**, 753–756.

Burnley, P., Green H. & Prior, D. 1991. Faulting associated with the olivine to spinel transformation in Mg_2GeO_4 and its implications for deep-focus earthquakes. *J. geophys. Res.* **96**, 425–443.

Buseck, P. R., Nord, G. L. & Veblen, D. R. 1980. Subsolidus phenomena in pyroxenes. In: *Reviews in Mineralogy, Volume* 7, *Pyroxenes* (edited by Prewitt, C. T.). Mineralogical Society of America, Michigan, 117–211.

Carpenter, M. A. & Salje, E. 1989. Time-dependent Landau theory for order/disorder processes in minerals. *Mineralog. Mag.* **53**, 483–504.

Castaing, J., Cadoz, J. & Kirby, S. H. 1981. Prismatic slip of Al_2O_3 single crystals below 1000°C in compression under hydrostatic pressure. *Am. Ceram. Soc.* **64**, 504–511.

Champness, P. E. & Lorimer, G. W. 1974. A direct lattice-resolution study of precipitation (exsolution) in orthopyroxenes. *Phil. Mag.* **30**, 357–366.

Christy, A. G. & Putnis, A. 1988. Planar and line defects in the sapphirine polytypes. *Phys. Chem. Miner.* **15**, 548–558.

Coe, R. S. 1970. The thermodynamic effect of shear stress on the ortho–clino inversion in enstatite and other coherent phase transitions characterized by a finite simple shear. *Contr. Miner. Petrol.* **26**, 247–264.

Coe, R. S. & Kirby, S. H. 1975. The orthoenstatite to clinoenstatite transformation by shearing and reversion by annealing: mechanism and potential applications. *Contr. Miner. Petrol.* **52**, 29–55.

Coe, R. S. & Müller, W. F. 1973. Crystallographic orientation of clinoenstatite produced by deformation of orthoenstatite. *Science* **180**, 64–66.

Coe, R. S. & Paterson, M. S. 1969. The α–β inversion in quartz: a coherent phase transition under nonhydrostatic stress. *J. geophys. Res.* **74**, 4921–4948.

Cohen, L. H. & Klement, W., Jr. 1967. High–low quartz inversions: determination to 35 kilobars. *J. geophys. Res.* **72**, 4245–4251.

Cohen, L. H. & Klement, W., Jr. 1976. Effect of pressure on reversible solid–solid transitions in nepheline and carnegieite. *Mineralog. Mag.* **40**, 487–492.

Cohen, L. H. & Klement, W., Jr. 1980. Tridymite: effect of hydro-

static pressure to 6 kbar on temperatures of two rapidly reversible transitions. *Contr. Miner. Petrol.* **71**, 401–405.

Dandurand, J. L., Gout, R. & Schott, J. 1982. Experiments on phase transformations and chemical reactions of mechanically activated minerals by grinding: petrogenetic implications. *Tectonophysics* **83**, 365–386.

D'Aragona, F. S., Delavignette, P. & Amelinckx, S. 1966. Direct evidence for the mechanism of the phase transition würtzite–sphalerite. *Phys. Stat. Sol.* **14**, K115–K118.

Darot, M., Gueguen, Y., Benchemam, Z. & Gaboriaud, R. 1985. Ductile–brittle transition investigated by micro-indentation: results for quartz and olivine. *Phys. Earth & Planet. Interiors* **40**, 180–186.

Dasgupta, D. R. 1963. The oriented transformation of aragonite into calcite. *Mineralog. Mag.* **33**, 924–928.

Depmeier, W. 1988. Aluminate sodalites—a family with strained structures and ferroic phase transitions. *Phys. Chem. Miner.* **15**, 419–426.

Dolino, G. 1985. Incommensurate phases of quartz. *Jap. J. appl. Phys.* **24**, Suppl. 24-2, 153–156.

Dolino, G. 1988. Incommensurate phase transitions in quartz and berlinite. In: *Structural and Magnetic Phase Transitions in Minerals* (edited by Ghose, S., Coey, J. M. D. & Salje, E.). Springer, New York, 17–38.

Dolino, G., Bachheimer, J. P., Berge, B., Zeyen, C. M. E., Van Tendeloo, G., Van Landuyt, J. & Amelinckx, S. 1984. Incommensurate phase of quartz: III. Study of the coexistence state between the incommensurate and the α-phase by neutron scattering and electron microscopy. *J. Physique* **45**, 901–912.

Dolino, G., Bastie, P., Berge, B., Vallade, M., Bethke, J., Regnault, L. P. & Zeyen, C. M. E. 1987. Stress induced $3q$–$1q$ incommensurate phase transition in quartz. *Europhys. Lett.* **3**, 601–609.

Doukhan, J. C. & Christie, J. M. 1982. Plastic deformation of sillimanite–Al_2SiO_5 single crystals under confining pressure and TEM investigation of the induced defect structure. *Bull. Minéral.* **105**, 583–589.

Doukhan, J. C., Doukhan, N., Koch, P. S. & Christie, J. M. 1985. Transmission electron microscopy investigation of lattice defects in Al_2SiO_5 polymorphs and plasticity induced polymorphic transformations. *Bull. Minéral.* **108**, 81–96.

Duclos, R. 1979. Study of the precipitation in $MgO \cdot 3.5Al_2O_3$ during creep experiments. *J. Physique* **40**, L109–L112.

Duclos, R., Doukhan, N. & Escaig, B. 1978. High temperature creep behaviour of nearly stoichiometric alumina spinel. *J. Mater. Sci.* **13**, 1740–1748.

Friend, C. M. & Miodownik, A. P. 1988. The calculation of stress-induced martensitic transformations in copper-base shape-memory alloys. In: *Phase Transformations* (edited by Lorimer, G. W.). Institute of Metals, London, 276–278.

Ghose, S., Van Tendeloo, G. & Amelinckx, S. 1988. Dynamics of a second-order phase transition: $P\bar{1}$ to $I\bar{1}$ transition in anorthite, $CaAl_2Si_2O_8$. *Science* **242**, 1539–1541.

Gillet, P. & Madon, M. 1982. Un model de dislocations pour le transition aragonite–calcite. *Bull. Minéral.* **105**, 590.

Green, H. & Burnley, P. 1989. A new self-organizing mechanism for deep-focus earthquakes. *Nature* **341**, 733–737.

Green, H. W., Young, T. E., Walker, D. & Scholz, C. H. 1990. Anticrack-associated faulting at very high pressure in natural olivine. *Nature* **348**, 720–722.

Grimm, H. & Dorner, B. 1975. On the mechanism of the α–β phase transformation of quartz. *J. Phys. Chem. Solids.* **36**, 407–413.

Hacker, B. R. & Kirby, S. H. 1993. High-pressure deformation of calcite marble and its transformation to aragonite under non-hydrostatic conditions. *J. Struct. Geol.* **15**, 1207–1222.

Halferdahl, L. B. 1961. Chloritoid: its composition, X-ray and optical properties, stability, and occurrence. *J. Petrol.* **2**, 49–135.

Hanscom, R. 1975. Refinement of the crystal structure of monoclinic chloritoid. *Acta cryst.* **B31**, 780–784.

Hanscom, R. 1980. The structure of triclinic chloritoid and chloritoid polymorphism. *Am. Mineral.* **65**, 534–539.

Hartley, N. E. W. & Wilshaw, T. R. 1973. Deformation and fracture of synthetic α-quartz. *J. Mater. Sci.* **8**, 265–278.

Hazen, R. M. 1976. Sanidine: predicted and observed monoclinic-to-triclinic reversible transformations at high pressure. *Science* **194**, 105–107.

Hemingway, B. S., Evans, H. T., Jr, Nord, G., Jr, Haselton, H. T., Jr, Robie, R. A. & McGee, J. J. 1986. Åkermanite: phase transitions in heat capacity and thermal expansion, and revised thermodynamic data. *Can. Mineral.* **24**, 425–434.

Henderson, C. M. B. & Thompson, A. B. 1980. The low-temperature inversion in sub-potassic nephelines. *Am. Mineral.* **65**, 970–980.

Heuer, A. H. & Nord, G. L. Jr. 1976. Polymorphic phase transitions in minerals. In: *Electron Microscopy in Mineralogy* (edited by Wenk, H.-R.). Springer, New York, 274–303.

Higgens, J. B., Ribbe, P. H. & Herd, R. K. 1979. Sapphirine I: crystal chemical contributions. *Contr. Miner. Petrol.* **68**, 349–356.

Hornstra, J. 1960. Dislocations, stacking faults and twins in the spinel structure. *J. Phys. Chem. Solids.* **15**, 311–323.

Kirby, S. H. 1976. The role of crystal defects in the shear-induced transformation of orthoenstatite to clinoenstatite. In: *Electron Microscopy in Mineralogy* (edited by Wenk, H.-R.). Springer, New York, 465–472.

Kirby, S. H. 1987. Localized polymorphic phase transformations in high-pressure faults and applications to the physical mechanism of deep earthquakes. *J. geophys. Res.* **92**, 13,798–13,800.

Kirby, S. H. & Christie, J. M. 1977. Mechanical twinning in diopside $Ca(Mg,Fe)Si_2O_6$. Structural mechanism and associated crystal defects. *Phys. Chem. Miner.* **1**, 137–163.

Kirby, S. H., Durham, W. B. & Stern, L. A. 1991. Mantle phase changes and deep-earthquake faulting in subducting lithosphere. *Science* **252**, 216–225.

Kirby, S. H., Durham, W. B. & Stern, L. A. 1992. The ice I–II transformation: mechanisms and kinetics under hydrostatic and nonhydrostatic conditions. In: *Physics and Chemistry of Ice* (edited by Maeno, N. & Hondoh, T.). Hokkaido University Press, Sapporo, 456–463.

Kirby, S. H. & Etheridge, M. A. 1981. Exsolution of Ca-clinopyroxene from orthopyroxene aided by deformation. *Phys. Chem. Miner.* **7**, 105–109.

Kirby, S. H., Hemingway, B. S. & Lee, R. 1990. Anomalous fracture and thermal behavior of hydrous minerals. *Am. Geophys. Un. Geophys. Monogr.* **56**, 119–126.

Kirby, S. H. & Veyssière, P. 1980. Plastic deformation of $MgO(Al_2O_3)_{1.1}$ spinel at $0.28T_m$: preliminary results. *Phil. Mag.* **A41**, 129–136.

Kohlstedt, D. L. & Vander Sande, J. B. 1976. On the detailed structure of ledges in an augite–enstatite interface. In: *Electron Microscopy in Mineralogy* (edited by Wenk, H.-R.). Springer, New York, 234–237.

Kriven, W. M. 1988. Possible alternative transformation tougheners to zirconia: crystallographic aspects. *J. Am Ceram. Soc.* **71**, 1021–1030.

Kriven, W. M., Fraser, W. L. & Kennedy, S. W. 1981. The martensite crystallography of tetragonal zirconia. In: *Advances in Ceramics, Volume 3, Science and Technology of Zirconia I* (edited by Heuer, A. H. & Hobbs, L. W.). American Ceramic Society, Columbus, Ohio, 82–97.

Kroll, H., Bambauer, H.-U. & Schirmer, U. 1980. The high albite–monalbite and analbite–monalbite transitions. *Am. Mineral.* **65**, 1192–1211.

Kronberg, M. L. 1957. Plastic deformation of single crystals of sapphire: basal slip and twinning. *Acta metall.* **5**, 507–523.

Kronenberg, A. K., Kirby, S. H. & Pinkston, J. 1990. Basal slip and mechanical anisotropy of biotite. *J. geophys. Res.* **95**, 19,257–19,278.

Lacam, A., Madon, M. & Poirier, J. P. 1980. Olivine glass and spinel formed in a laser heated, diamond anvil high pressure cell. *Nature* **288**, 155–157.

Lange, R. A., Carmichael, I. S. E. & Stebbins, J. F. 1986. Phase transitions in leucite ($KAlSi_2O_6$), orthorhombic $KAlSiO_4$, and their iron analogues ($KFeSi_2O_6$, $KFeSiO_4$). *Am. Mineral.* **71**, 937–945.

Langer, K. & Schreyer, W. 1969. Infrared and powder X-ray diffraction studies on the polymorphism of cordierite, $Mg_2(Al_4Si_5O_{18})$. *Am. Mineral.* **54**, 1442–1459.

Lee, W. E. & Heuer, A. H. 1987. On the polymorphism of enstatite. *J. Am. Ceram. Soc.* **70**, 349–360.

Lee, R. W. & Kirby, S. H. 1984. Experimental deformation of topaz crystals: possible embrittlement by intracrystalline water. *J. geophys. Res.* **89**, 4161–4166.

Linker, M. F. & Kirby, S. H. 1981. Anisotropy in the rheology of hydrolytically weakened synthetic quartz crystals. *Am. Geophys. Un. Geophys. Monogr.* **24**, 29–48.

Liu, M. & Yund, R. A. 1992. NaSi–CaAl interdiffusion in plagioclase. *Am. Mineral.* **77**, 275–283.

Lorimer, G. W. (editor) 1988. *Phase Transformations*. Institute of Metals, London.

Madon, M. & Poirier, J. P. 1983. Transmission electron microscope observations of α, β, and γ $(Mg,Fe)_2SiO_4$ in shocked meteorites: planar defects and polymorphic transitions. *Phys. Earth & Planet. Interiors* **33**, 31–44.

Mardix, S. 1986. Polytypism: a controlled thermodynamic phenomenon. *Phys. Rev.* **B33**, 8677–8684.

Mardix, S., Kalman, Z. H. & Steinberger, I. T. 1968. Periodic slip processes and the formation of polytypes in zinc sulphide crystals. *Acta cryst.* **A24**, 464–469.

Mardix, S., Lang, A. R., Kowalski, G. & Makepeace, A. P. W. 1987. On structure and twist in ZnS crystal whiskers. *Phil. Mag.* **56**, 251–261.

Mardix, S. & Steinberger, I. T. 1970. Tilt and structure transformation in ZnS. *J. appl. Phys.* **41**, 5339–5341.

Mares, V. M. & Kronenberg, A. K. 1993. Experimental deformation of muscovite. *J. Struct. Geol.* **15**, 1061–1075.

McLaren, A. C. & Etheridge, M. A. 1976. A transmission electron microscope study of naturally deformed orthopyroxene. I. Slip mechanisms. *Contr. Miner. Petrol.* **57**, 163–177.

Merrill, L. & Bassett, W. A. 1975. Crystal structure of $CaCO_3$(II), a high-pressure metastable phase of calcium carbonate. *Acta cryst.* **B31**, 343–349.

Michalske, T. A. & Freiman, S. W. 1983. A molecular interpretation for stress corrosion in vitreous silica. *J. Am. Ceram. Soc.* **66**, 284–288.

Mori, H. & Takeda, H. 1988. Stress induced transformation of pigeonites from achondritic meteorites. *Phys. Chem. Miner.* **15**, 252–259.

Nord, G. L., Heuer, A. H. & Lally, J. S. 1976. Pigeonite exsolution from augite. In: *Electron Microscopy in Mineralogy* (edited by Wenk, H.-R.). Springer, New York, 220–227.

Nukui, A., Nakazawa, H. & Akao, M. 1978. Thermal changes in monoclinic tridymite. *Am. Mineral.* **63**, 1252–1259.

Palmer, D. C., Putnis, A. & Salje, E. K. H. 1988. Twinning in tetragonal leucite. *Phys. Chem. Miner.* **16**, 298–303.

Palmer, D. C., Salje, E. K. H. & Schmahl, W. W. 1989. Phase transitions in leucite: X-ray diffraction studies. *Phys. Chem. Miner.* **16**, 714–719.

Patel, J. & Cohen, M. 1953. Criterion for the action of applied stress in the martensitic transformation. *Acta. metall.* **1**, 531–538.

Paterson, M. S. 1973. Nonhydrostatic thermodynamics and its geologic applications. *Rev. Geophys. & Space Phys.* **11**, 355–389.

Paterson, M. S. & Weaver, C. W. 1970. Deformation of polycrystalline MgO under pressure. *J. Am. Ceram. Soc.* **53**, 463–471.

Poirier, J. P. 1981. Martensitic olivine-spinel transformation and plasticity of the mantle transition zone. In: *Anelasticity in the Earth* (edited by Stacey, F. D., Paterson, M. S. & Nicholas, A.). *Am. Geophys, Un. Geodyn. Ser.* **4**, 113–117.

Poirier, J. P. 1985. *Creep of Crystals.* Cambridge University Press, Cambridge, U.K.

Porter, D. A. & Easterling, K. E. 1981. *Phase Transformations in Metals and Alloys.* Van Nostrand Reinhold, Berkshire.

Price, G. D., Putnis, A. & Smith, D. G. W. 1982. A spinel to β-phase transformation mechanism in $(Mg,Fe)_2SiO_4$. *Nature* **296**, 729–731.

Putnis, A. & McConnell, J. D. C. 1980. *Principles of Mineral Behaviour.* Elsevier, New York.

Putnis, A., Salje, E., Redfern, S. A. T., Fyfe, C. A. & Strobl, H. 1987. Structural states of Mg-cordierite I: order parameters from synchrotron X-ray and NMR data. *Phys. Chem. Miner.* **14**, 446–454.

Raleigh, C. B. & Paterson, M. S. 1965. Experimental deformation of serpentinite and its tectonic implications. *J. geophys. Res.* **70**, 3965–3985.

Ray, N. J., Putnis, A. & Gillet, P. 1986. Polytypic relationship between clinozoisite and zoisite. *Bull. Minéral.* **109**, 667–685.

Roy, D. M., Roy, R. & Osborn, E. F. 1953. *J. Am. Ceram. Soc.* **36**, 149.

Reeder, R. J., Redfern, S. A. T. & Salje, E. 1988. Spontaneous strain at the structural phase transition in $NaNO_3$. *Phys. Chem. Miner.* **15**, 605–611.

Robin, P.-Y. F. 1974. Thermodynamic equilibrium across a coherent interface in a stressed crystal. *Am. Mineral.* **59**, 1286–1298.

Ross, M. & Huebner, J. S. 1979. Temperature-composition relationships between naturally occurring augite, pigeonite, and orthopyroxene at one bar pressure. *Am. Mineral.* **64**, 1133–1155.

Rubie, D. C. 1983. Reaction-enhanced ductility: the role of solid–solid univariant reactions in deformation of the crust and mantle. *Tectonophysics* **96**, 331–352.

Rubie, D. C. 1990. Mechanisms of reaction-enhanced deformability in minerals and rocks. In: *Deformation Processes in Minerals, Ceramics, and Rocks* (edited by Barber, D. J. & Meredith, P. G.). Unwin Hyman, London, 262–295.

Rubie, D. C. & Brearley, A. J. 1990. Mechanism of the γ–β phase transformation of Mg_2SiO_4 at high temperature and pressure. *Nature* **348**, 628–631.

Rubie, D. C. & Thompson, A. B. 1985. Kinetics of metamorphic reactions at elevated temperatures and pressures: an appraisal of available experimental data. In: *Metamorphic Reactions. Kinetics, Textures and Deformation* (edited Thompson, A. B. & Rubie, D. C.). Springer, New York, 27–79.

Rutter, E. H. & Brodie, K. H. 1988. Experimental syntectonic dehydration of serpentinite under conditions of controlled pore water pressure. *J. geophys. Res.* **93**, 4907–4932.

Sammis, C. G. 1989. Rock deformation: stress-induced segregation. *Nature* **338**, 114–115.

Seifert, F., Czank, M., Simons, B. & Schmahl, W. 1987. A commensurate-incommensurate phase transition in iron-bearing Åkermanites. *Phys. Chem. Miner.* **14**, 26–35.

Simons, P. Y. & Dachille, F. 1970. Possible topotaxy in the TiO_2 system. *Am Mineral.* **55**, 403–415.

Sirotin, Y. I. & Shaskolskya, M. P. 1982. *Fundamentals of Crystal Physics.* Mir, Moscow.

Smelik, E. A. & Veblen, D. R. 1992. Exsolution of hornblende and the solubility limits of calcium in orthoamphibole. *Science* **257**, 1669–1672.

Smith, D. L. & Evans, B. 1984. Diffusion crack healing in quartz. *J. geophys. Res.* **89**, 4125–4136.

Smith, J. V. 1969. Magnesium pyroxenes at high temperature: inversion in clinoenstatite. *Nature* **222**, 256–257.

Smyth, J. R. 1974. Experimental study on the polymorphism of enstatite. *Am. Mineral.* **59**, 345–352.

Smyth, J. R. & Burnham, C. W. 1972. The crystal structures of high and low clinohypersthene. *Earth Planet. Sci. Lett.* **14**, 183–189.

Snoeck, E., Roucau, C. & Saint-Gregoire, P. 1986. Electron microscopy study of the modulated phases in berlinite $AlPO_4$ and quartz. *J. Physique* **47**, 2041–2053.

Sueno, S., Prewitt, C. T. & Kimata, M. 1985. Structural aspects of phase transitions in Fe–Mg–Ca pyroxenes. *Am. Mineral.* **70**, 141–148.

Swain, M. V., Williams, J. S., Lawn, B. R. & Beek, J. J. H. 1973. A comparative study of the fracture of various silica modifications using the Hertzian test. *J. Mater. Sci.* **8**, 1153–1164.

Thompson, A. B. & Wennemer, M. 1979. Heat capacities and inversions in tridymite, cristobalite, and tridymite–cristobalite mixed phases. *Am. Mineral.* **64**, 1018–1026.

Tingle, T. N., Green, H. W., II, Scholz, C. H. & Koczynski, T. A. 1993. The rheology of faults triggered by the olivine–spinel transformation in Mg_2GeO_4 and its implications for the mechanism of deep-focus earthquakes. *J. Struct. Geol.* **15**, 1249–1256.

Trojer, F. J. 1968. The crystal structure of parawollastonite. *Z. Kristallogr.* **127**, 291–308.

Trommsdorff, V. & Wenk, H.-R. 1968. Terrestrial metamorphic clinoenstatite in kinks of bronzite crystals. *Contr. Miner. Petrol.* **19**, 158–168.

Turner, F. J., Heard, H. & Griggs, D. T. 1960. Experimental deformation of enstatite and accompanying transformation to clinoenstatite. *21st. Geol. Congr.* **18**, 399–408.

Van Goethem, L., Van Landuyt, J. & Amelinckx, S. 1977. The α–β transition in amethyst quartz as studied by electron microscopy and diffraction. *Phys. Stat. Sol. (a)* **41**, 129–137.

Van Landuyt, J., Van Tendeloo, G., Amelinckx, S. & Walker, M. B. 1985. Interpretation of Dauphiné-twin-domain configurations resulting from the α–β phase transition in quartz and aluminum phosphate. *Phys. Rev.* **B31**, 2986–2992.

Van Tendeloo, G., Van Landuyt, J. & Amelinckx, S. 1976. The α–β phase transition in quartz and $AlPO_4$ as studied by electron microscopy and diffraction. *Phys. Stat. Sol. (a)* **33**, 723–735.

Veyssière, P. 1988. Dislocation core effects in plasticity. *Rev. Phys. Appl.* **23**, 431–443.

Veyssière, P. 1977. Unpublished thèse de Doctorat, Université de Poitiers.

Veyssière, P. & Carter, C. B. 1988. Dissociation of dislocations in $MgAl_2O_4$ spinel deformed at low temperatures. *Phil. Mag. Lett.* **57**, 211–220.

Veyssière, P., Kirby, S. H. & Rabier, J. 1980. Plastic deformation of $MgO{:}nAl_2O_3$ spinels at temperatures below 1000°C (0.5 T_m). *J. Physique* **41**, 175–178.

Wenk, H.-R. 1969. Polymorphism of wollastonite. *Contr. Miner. Petrol.* **22**, 238–247.

Wenk, H.-R., Muller, W. F., Liddell, N. A., & Phakey, P. P. 1976. Polytypism in wollastonite. In: *Electron Microscopy in Mineralogy* (edited by Wenk, H.-R.). Springer, New York, 324–331.

Wheeler, J. 1987. The significance of grain-scale stresses in the kinetics of metamorphism. *Contr. Miner. Petrol.* **97**, 397–404.

White, S. H. & Knipe, R. J. 1978. Transformation and reaction enhanced ductility in rocks. *J. geol. Soc. Lond.* **135**, 513–516.

Wiederhorn, S. M. 1978. Mechanisms of subcritical crack growth in glass. *Fract. Mech. Ceram.* **4**. 549–580.

Wood, B. J., Kirkpatrick, R. J. & Montez, B. 1986. Order–disorder in $MgAl_2O_4$ spinel. *Am. Mineral.* **71**, 999–1006.

Yund, R. A. & Tullis, J. 1983a. Strained cell parameters for coherent lamellae in alkali feldspars and iron-free pyroxenes. *Neues Jb. Miner. Mh.* **H1**, 22–34.

Yund, R. A. & Tullis, J. 1983b. Subsolidus phase relations in the alkali feldspars with emphasis on coherent phases. In: *Reviews in Mineralogy, Volume* 2, *Feldspar Mineralogy* (edited by Ribbe, P. H.). Mineralogical Society of America, Michigan, 141–176.